CELL BIOLOGY

DNA dioxygenases Tet2/3 regulate gene promoter accessibility and chromatin topology in lineage-specific loci to control epithelial differentiation

Guo-Dong Chen[1]†, Iqra Fatima[1], Qin Xu[2], Elena Rozhkova[1], Michael Y. Fessing[3], Andrei N. Mardaryev[3], Andrey A. Sharov[1], Guo-Liang Xu[2,4]†, Vladimir A. Botchkarev[1]†*

Execution of lineage-specific differentiation programs requires tight coordination between many regulators including Ten-eleven translocation (TET) family enzymes, catalyzing 5-methylcytosine oxidation in DNA. Here, by using *Keratin 14–Cre*–driven ablation of *Tet* genes in skin epithelial cells, we demonstrate that ablation of *Tet2/Tet3* results in marked alterations of hair shape and length followed by hair loss. We show that, through DNA demethylation, *Tet2/Tet3* control chromatin accessibility and Dlx3 binding and promoter activity of the *Krt25* and *Krt28* genes regulating hair shape, as well as regulate interactions between the *Krt28* gene promoter and distal enhancer. Moreover, *Tet2/Tet3* also control three-dimensional chromatin topology in Keratin type I/II gene loci via DNA methylation–independent mechanisms. These data demonstrate the essential roles for Tet2/3 in establishment of lineage-specific gene expression program and control of Dlx3/Krt25/Krt28 axis in hair follicle epithelial cells and implicate modulation of DNA methylation as a novel approach for hair growth control.

INTRODUCTION

Differentiation of stem cells into specialized cell lineages is accompanied by establishment of the distinct patterns of gene activation and silencing regulated at several levels including signaling molecules, transcription factors, and epigenetic machinery (*1*–*6*). Lineage-specific and functionally related genes frequently form conserved clusters or loci in the mammalian genomes (*7*, *8*). In the mouse genome, there are more than 30 such large (more than 0.5 Mbp) lineage-specific gene loci containing at least 10 functionally related genes (*7*–*9*). Many lineage-specific gene loci belong to distinct topologically associating domains (TADs), defined as the chromatin domains with higher frequency of spatial contacts within the domains compared to the regions across TAD borders (*10*). The detailed chromosome conformation capture analysis of several lineage-specific gene loci revealed the importance of their proper spatial organization in executing lineage-specific gene expression programs by establishment of distinct enhancer-promoter interactions networks within individual TADs, as well as between neighboring TADs (*9*, *11*).

DNA methylation and subsequent oxidation of 5-methylcytosine (5mC) into 5-hydroxymethylcytosine (5hmC) are key epigenetic events regulating development and stem cell differentiation in mammals (*12*–*14*). The process of 5mC conversion toward unmethylated state also includes formation of 5-formylcytosine and 5-carboxycytosine (*15*). Oxidation of 5-mC is catalyzed by the Ten-eleven translocation (Tet) family enzymes (Tet1/2/3) and serve as an important step in DNA demethylation (*16*). In addition to 5-mC oxidation at gene regulatory regions and Cytosine-phosphate-Guanine (CpG) islands, Tet proteins are also capable of positively regulating gene transcription by activating enhancers via DNA demethylation (*14*, *17*). However, the role of Tet enzymes in the control of gene expression at the levels of lineage-specific gene loci occupying individual TADs remains to be explored.

Skin epithelial cells serve as an attractive model for studying mechanisms controlling differentiation-associated chromatin remodeling: Keratinocyte-specific genes are organized in the genome into three distinct loci [Epidermal Differentiation Complex (EDC) locus and Keratin type I/II loci] located on mouse chromosomes 3, 11, and 15, respectively (*18*–*20*). Whereas the 3.1-Mb EDC locus is spread among four neighboring TADs (*9*), Keratin type I/II loci are relatively smaller (about 0.9 and 0.7 Mb, respectively) and belong to individual TADs, harboring more than 60 epithelial and hair keratin genes (*21*).

During development, epithelial skin stem cells differentiate and form epidermis, a stratified self-renewing epithelium, as well as a number of appendages including hair follicles (HFs) (*22*). Terminal differentiation of epidermal cells is accompanied by sequential changes in expression of the genes encoding epidermal keratins (*Krt1*, *Krt5*, *Krt10*, and *Krt14*) in the Keratin type I/II loci, followed by the onset of gene expression in EDC locus resulting in a formation of the epidermal barrier (*23*, *24*). In the HF, terminal keratinocyte differentiation is accompanied by activation of the different sets of genes encoding hair shaft–specific and inner root sheath (IRS)–specific keratins (*Krt25* to *Krt28*, *Krt31* to *Krt37*, and *Krt81* to *Krt86*), while expression of epidermal keratin genes is down-regulated (*25*).

In skin epithelial cells, DNA methylation of the genes activated during terminal differentiation is progressively decreased (*26*). In accordance with this, inactivation of *DNMT1* in human epidermis results in premature onset of expression of terminal differentiation genes, as well as in decrease of cell proliferation associated with increased expression of cell cycle inhibitors p15/Cyclin-dependent

[1]Department of Dermatology, Boston University, Boston, MA, USA. [2]State Key Laboratory of Molecular Biology, Shanghai Institute of Biochemistry and Cell Biology, Center for Excellence in Molecular Cell Science, Chinese Academy of Sciences, Shanghai, China. [3]Centre for Skin Sciences, School of Chemistry and Biosciences, University of Bradford, Bradford, UK. [4]Shanghai Key Laboratory of Medical Epigenetics, Institutes of Biomedical Sciences, Medical College of Fudan University, Shanghai, China.
†These authors contributed equally to this work.
*Corresponding author. Email: vladbotc@bu.edu

kinase 4 inhibitor B (INK4B) and p16/Cyclin-dependent kinase 4 inhibitor A (INK4A) (*27*). In mouse HF, ablation of *Dnmt1* gene leads to decrease of cell proliferation in the hair matrix and results in hair loss (*28*). However, the role of Tet enzymes in the control of lineage-specific gene expression in the Keratin type I/II loci during terminal differentiation remains to be explored.

Here, we demonstrate that Tet2/3 enzymes play a key role in the control of gene expression in lineage-specific gene loci via regulating promoter accessibility and three-dimensional chromatin landscape in terminally differentiating HF keratinocytes. These data highlight the role of Tet-mediated DNA demethylation in establishment of lineage-specific gene expression program in epithelial cells and implicate modulation of Tet activity as a novel approach for hair growth control.

RESULTS

Tet2 and *Tet3* contribute to 5hmC oxidation at active promoters and enhancers in skin epithelial cells

To define a relevance of the Tet enzymes to the control of gene expression in skin epithelial cells, we first used the Cleavage Under Targets and Tagmentation (CUT&Tag) assay and analyzed the distribution of 5hmC as the Tet1/2/3-mediated DNA oxidation product in the genome of primary mouse keratinocytes (Fig. 1, A and B). We correlated 5hmC data with the positions of active promoters and enhancers depicted by CUT&Tag analyses of H3K4me3 and H3K27ac/H3K4me1 histone marks, respectively. We found that, in the keratinocyte genome, 5hmC peaks show significant enrichment at the active gene promoters and enhancers including the epithelial keratin genes that constitute Keratin type I/II loci (Fig. 1, A and B).

Next, we used RNA sequencing (RNA-seq) analyses to define expression of the distinct Tet enzymes in primary mouse keratinocytes, as well as in basal epidermal keratinocytes and HF matrix keratinocytes fluorescence-activated cell sorting (FACS)–sorted from mouse skin at postnatal day 4.5 (P4.5). Consistent with the data published previously (*29*, *30*), *Tet2* and *Tet3* transcripts showed much higher expression levels compared to *Tet1* in all three populations of keratinocytes (Fig. 1C and fig. S1, A and B). In concordance to RNA-seq data, immunofluorescence analyses revealed that Tet2 and Tet3 proteins showed higher expression levels in the developing skin and HFs compared to Tet1 (Fig. 1, D to F). Tet2 and Tet3 were expressed in the developing epidermis and HF placodes [embryonic day 18.5 (E18.5)], in HF outer root sheath, and in differentiating hair matrix keratinocytes and dermal papilla (Fig. 1, E and F). Differentiating epidermal and hair matrix keratinocytes also contained strong 5hmC immunofluorescence (Fig. 1G and fig. S1C), thus implicating Tet2/3 involvement in the control of terminal differentiation of skin epithelial cells. Double immunovisualization of Tet2 or Tet3 and markers of the keratinocytes of the IRS and hair shaft (AE13 and AE15) or hair matrix keratinocytes (Ephrin-B1) revealed colocalization of these proteins in differentiating epithelial cells of the HF (Fig. 1, E and F, and fig. S1D). However, lack of the detectable levels of Tet2 and Tet3 were seen in the HF bulge, harboring epithelial stem cells and showing elevated expression of the stem cell marker Lhx2 (fig. S1E) (*31*–*33*).

Krt14-Cre–mediated *Tet1/2/3* ablation leads to alterations in hair growth

Genetically engineered mice with single or simultaneous ablation of *Tet1* and *Tet2* do not exhibit any visible abnormalities in skin or hair morphology, while *Tet3* knockout mice show neonatal lethality (*34*–*36*). To exclude the potential redundancy in activities of *Tet* genes and explore their roles in the control of keratinocyte differentiation, we crossed *Krt14-Cre* mice with $Tet2^{fl/fl}/Tet3^{fl/fl}$ mice (*37*, *38*) to simultaneously ablate *Tet2* and *Tet3* genes in keratinocytes (*Krt14-Cre*/$Tet2^{fl/fl}/Tet3^{fl/fl}$ double knockout or TetDKO mice). In addition, we crossed *Krt14-Cre* mice with $Tet1^{fl/fl}/Tet2^{fl/fl}/Tet3^{fl/fl}$ mice (*39*) to ablate all three *Tet* genes in the Krt14-expressing cells (*Krt14-Cre*/$Tet1^{fl/fl}/Tet2^{fl/fl}/Tet3^{fl/fl}$ triple knockout or TetTKO mice) (Fig. 2, A and B, and fig. S2A). Because $Tet2^{fl/fl}/Tet3^{fl/fl}$ mice were generated via targeting the exons 3 or 8 of the *Tet2* or *Tet3* genes, respectively (*37*, *38*), while $Tet1^{fl/fl}/Tet2^{fl/fl}/Tet3^{fl/fl}$ mice were generated by using different targeting strategy including the ablation of the exons 9 to 11 of all three *Tet* genes (*39*), we used this opportunity to compare the similarities and differences in the skin phenotypes between TetTKO mice and two different TetDKO mice (TetDKO mice generated independently and TetDKOT mice obtained as a part of generation of the triple knockout TetTKO mice) (fig. S2, A and B).

RNA-seq analyses of primary keratinocytes from wild-type (WT), TetDKO, and TetTKO mice confirmed ablations of the corresponding exons of *Tet1*, *Tet2*, and *Tet3* genes (Fig. 2, A and B). To confirm the *Krt14*-Cre–driven ablation of *Tet* genes in situ, immunofluorescence analyses of 5hmC was performed and revealed a lack of 5hmC in the epidermal and hair matrix keratinocytes of TetDKO and TetTKO mice (Fig. 2G and fig. S2). However, 5hmC levels in the dermis or in the dermal papilla of the HFs were unaltered in TetDKO and TetTKO mice, thus serving as internal controls for epithelial-specific *Tet1/Tet2/Tet3* ablations (Fig. 2G and fig. S2).

TetDKO and TetTKO newborn mice were smaller compared to WT littermates (fig. S2D). At P1.5, the number of HFs in the back skin of TetDKO and TetTKO mice, as well as the rate of their morphogenesis, was quite similar to the corresponding WT controls (fig. S2, G and H). In contrast to TetDKO mice, the epidermis of P1.5 TetTKO mice was significantly thinner compared to WT controls (fig. S2, G and H).

During postnatal development, animals of the all three mutant strains generated (TetDKO, TetDKOT, and TetTKO mice) remained smaller compared to age-matched WT controls (fig. S2E) and exhibited notable similarities in the skin phenotype including marked alterations of the hair growth and relatively minor changes in the epidermis (Fig. 2, C and D, and figs. S2F and S3, C to E). TetDKO, TetDKOT, and TetTKO mice showed appearance of sparce and short hairs on the back compared to age-matched WT mice, followed by hair loss occurring between P20 and P39 (Fig. 2, C and D, and fig. S2, E and F). TetTKO mice died at about P40 due to unidentified reasons, while TetDKO mice after P45 to P50 showed development of cycling alopecia and were completely deprived of pelage hairs by 7 months of age (Fig. 2C).

Analyses of the hair shafts plucked from TetDKO and TetTKO mice at about P20 to P24 revealed marked alterations of the hair length and shape: Compared to WT controls, hairs in TetDKO and TetTKO mice were significantly shorter and exhibited curly phenotype with a lack of bending specifying distinct hair types (guard, awl, auchen, and zigzag) in normal mouse fur (Fig. 2, C, E, F, H, and I) (*40*, *41*).

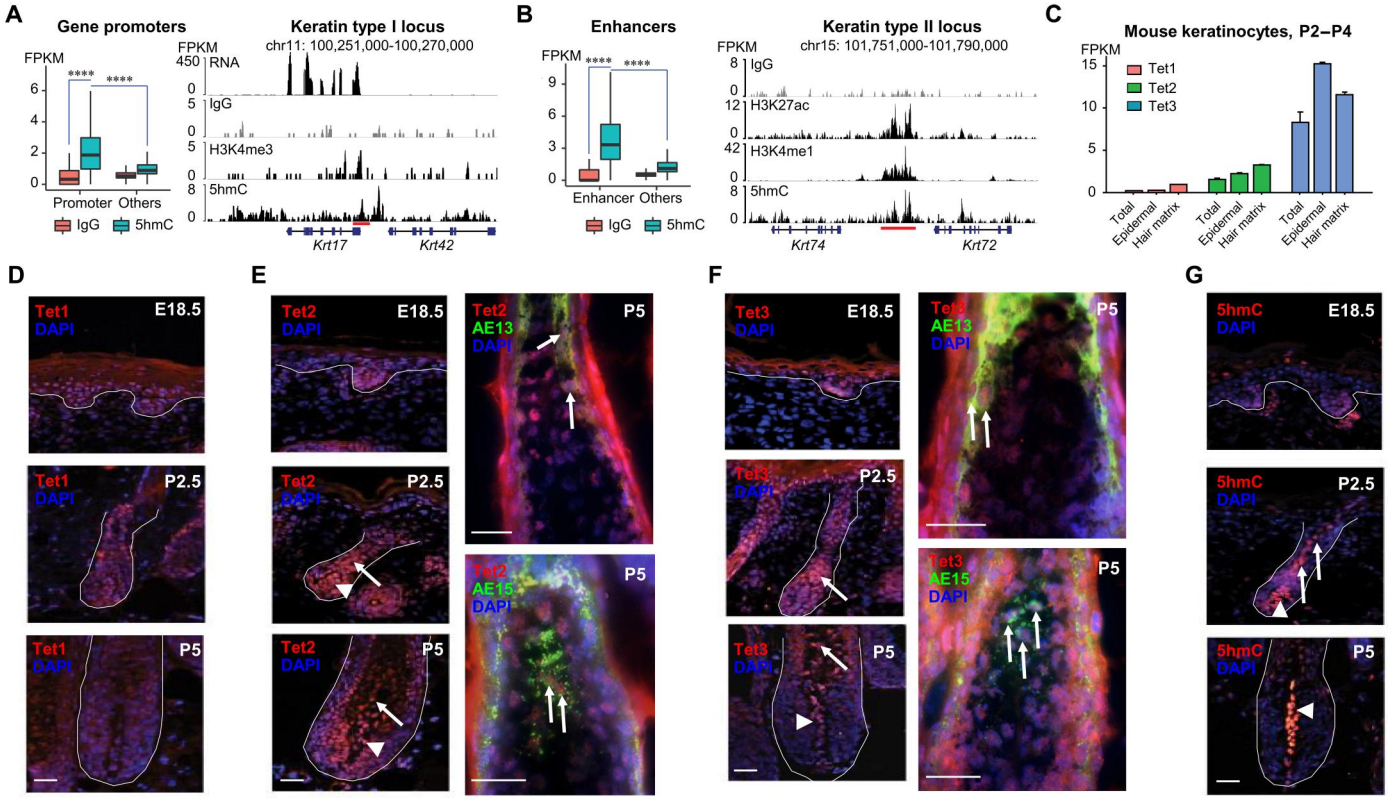

Fig. 1. 5hmC is enriched at gene promoters and enhancers in keratinocytes, while Tet1/2/3 expressions show dynamic changes in mouse skin and HF during embryonic and early postnatal development. (**A** and **B**) CUT&Tag analyses show enrichment of the normalized 5hmC levels at gene promoters (A) and enhancers (B) in primary mouse keratinocytes. Specific examples of the tracks (5hmc, H3K4me3, H3K4me1, and H3K27ac) demonstrate 5hmC peaks (highlighted) at the promoter of *Krt17* gene [(A) Keratin type I locus] and at the enhancer located between *Krt72* and *Krt74* genes [(B) Keratin type II locus] Data are presented as means ± SD. ****$P \leq 0.001$. FPKM, fragments per kilobase; IgG, immunoglobulin G. (**C**) RNA sequencing (RNA-seq) data for *Tet1*, *Tet2*, and *Tet3* in primary epidermal keratinocytes and fluorescence-activated cell sorting (FACS)–sorted basal epidermal and hair matrix keratinocytes isolated from mouse skin at postnatal day 2 (P2) to P4. (**D** to **G**) Immunofluorescent visualization of Tet1 (D), Tet2 (E), Tet3 (F), and 5hmC (G) in mouse skin at embryonic day 18.5 (E18.5), P2.5, and P5. Tet2, Tet3, and 5hmC are expressed in differentiating hair shaft keratinocytes (arrows) and in the dermal papillae (arrowheads). Covisualization of Tet2 or Tet3 and markers of the inner root sheath/hair shaft (AE13 and AE15) show expressions of the Tet2 (E) and Tet3 (F) in differentiating IRS and hair shaft keratinocytes (arrows). White lines demarcate the epidermal-dermal border and the HF. Sections are counterstained with 4′,6-diamidino-2-phenylindole (DAPI; blue). Scale bars, 25 μm.

Histologically, HFs in TetDKO and TetTKO mice showed a similar size of the hair bulb compared to WT controls (Fig. 2, H and I) and exhibited a slower catagen-telogen-anagen progression (Fig. 3A). Hair matrix keratinocytes in TetDKO and TetTKO mice showed significantly reduced proliferation compared to WT controls (Fig. 3B and fig. S3, A and B). In contrast to WT mice, hair matrix keratinocytes in TetDKO mice also showed marked down-regulation of the Krt25, an important component of the HF IRS regulating hair shape (Fig. 3C) (*42*). In addition, marked decrease in expression of another IRS component trichohyalin (depicted by AE15 antibody) was seen in the HFs of TetDKO mice compared to WT controls (Fig. 3D). Similarly to the IRS-specific markers, decrease in expression of the hair shaft–specific keratins visualized by the AE13 antibody was seen in TetDKO mice versus the controls (Fig. 3E and fig. S3B).

However, Krt14 expression was significantly increased in the hair matrix keratinocytes upon *Tet2/Tet3* ablations: In WT HFs, Krt14 was expressed in the outer root sheath and unilaterally in the hair matrix keratinocytes, while in TetDKO mice, a strong bilateral Krt14 expression was seen in the hair matrix in addition to the outer root sheath (Fig. 3F). In contrast to the HFs, lack of visible differences in the Krt14, Krt10, and loricirin expressions was seen between the epidermis of WT and TetDKO mice (fig. S3, C to E).

Tet2/3-deficient hair matrix keratinocytes show altered expression of differentiation-related genes

Because TetDKO, TetDKOT, and TetTKO mice showed alterations of hair structure and shape as a major skin phenotype occurring upon ablations of *Tet* genes, we focused on the mechanisms underlying the control of hair-specific keratinocyte differentiation. TetDKO model was used primarily due to a larger size of the animals and better opportunity to collect a sufficient number of cells required for analyses, compared to TetTKO mice. Ephrin-B1$^+$ population of hair matrix keratinocytes (*43*) were FACS-sorted from the P4.5 control and TetDKO mice for RNA isolation and RNA-seq analyses (Fig. 4A and fig. S4A). EphB1$^+$ keratinocytes isolated from TetDKO mice did not show any increase in the levels of *Tet1* or *EphB1* transcripts and proteins compared to WT controls (fig. S4, C to E), thus supporting a feasibility for using this cell population for further analyses.

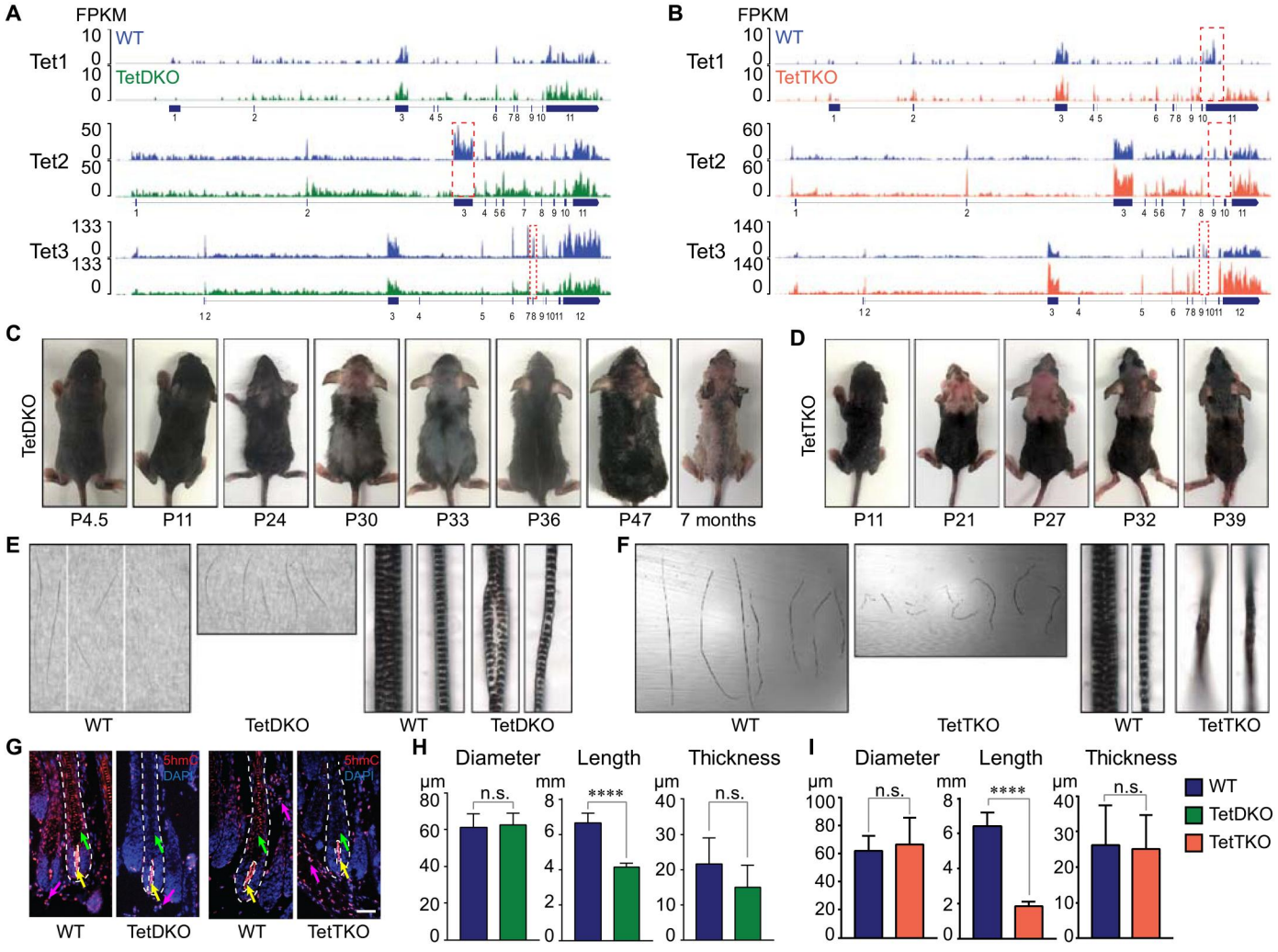

Fig. 2. Skin and hair phenotypes of Tet DKO and Tet TKO mice. (**A** and **B**) RNA-seq tracks of *Tet1*, *Tet2*, and *Tet3* in primary keratinocytes of TetDKO (A, green) and TetTKO (B, tomato) mice. Lack of the transcripts at the exons 3 and 8 of the *Tet2* and *Tet3* genes, respectively, is highlighted by red dotted line (A). Lack of the transcripts at the exons 9 to 11 of the *Tet1*, *Tet2*, and *Tet3* genes is highlighted by red dotted line (B). *Y* value is FPKM. (**C** and **D**) Images of TetDKO and TetTKO mice at different time points of postnatal development. Sparse and woolly fur and hair loss developed between P21 and P39 are seen in TetDKO and TetTKO mice. (**E** and **F**) Hair shafts of wild-type (WT), Tet DKO, and Tet TKO mice. Short and curly hair with a lack of bending are seen in both TetDKO and TetTKO mice. Hair shaft lesions and spindle-shaped hair shafts are seen in TetDKO and TetTKO mice, respectively. (**G**) Immunofluorescence staining for 5hmC (red) in the HFs of WT, TetDKO, and TetTKO mice. 5hmC signals decreased significantly in the HF epithelium (green arrows) but not in the HF dermal papilla (yellow arrows) or interfollicular dermis (pink arrows) of TetDKO and TetTKO mice. Cell nuclei are counterstained by DAPI. (**H** and **I**) Hair bulb diameter (P11), hair shaft length (P24), and thickness (P24) in WT, TetDKO, and TetTKO mice. Decreased hair shaft length is seen in TetDKO and TetTKO mice. Lack of significant changes in the hair bulb diameter and hair shaft thickness in mutant mice compared to WT controls. Data are presented as means ± SD. ****$P \leq 0.0001$; Student's *t* test. n.s., not significant. Scale bar, 50 μm

RNA-seq data revealed >2-fold differences in expression of 522 genes between WT and TetDKO mice with a strong enrichment of the genes involved in the control of keratinocyte differentiation, HF development, and cycling (Fig. 4, B to D, and fig. S4B). Vast majority of genes in these categories belong to the Keratin type I/II loci, and among the genes down-regulated in hair matrix keratinocytes of TetDKO mice were *Krt25* and *Krt28* encoding the IRS-specific keratins regulating hair shape (Fig. 4, B and C, and table S1).

On the other hand, together with other genes encoding the IRS-specific (*Krt27*, *Krt71*, and *Krt73*) and hair shaft–specific keratins (*Krt31*, *Krt33a*, *Krt35*, *Krt81*, *Krt83*, and *Krt86*), *Krt14* gene normally expressed at high levels in basal epidermal layer and HF outer root sheath was also up-regulated in hair matrix keratinocytes of TetDKO mice (Fig. 4, B and C, and table S1). Down-regulation of *Krt25* and up-regulation of the *Krt14* transcripts were consistent with the immunofluorescence analysis results of Krt25 or K14 protein expressions in the HF matrix of TetDKO mice (Fig. 3, C and F). In addition to keratin genes, *Foxn1* and *Hoxc13* genes encoding transcription factors controlling keratin gene expression in the HF were up-regulated in TetDKO mice (Fig. 4, B and C, and table S1).

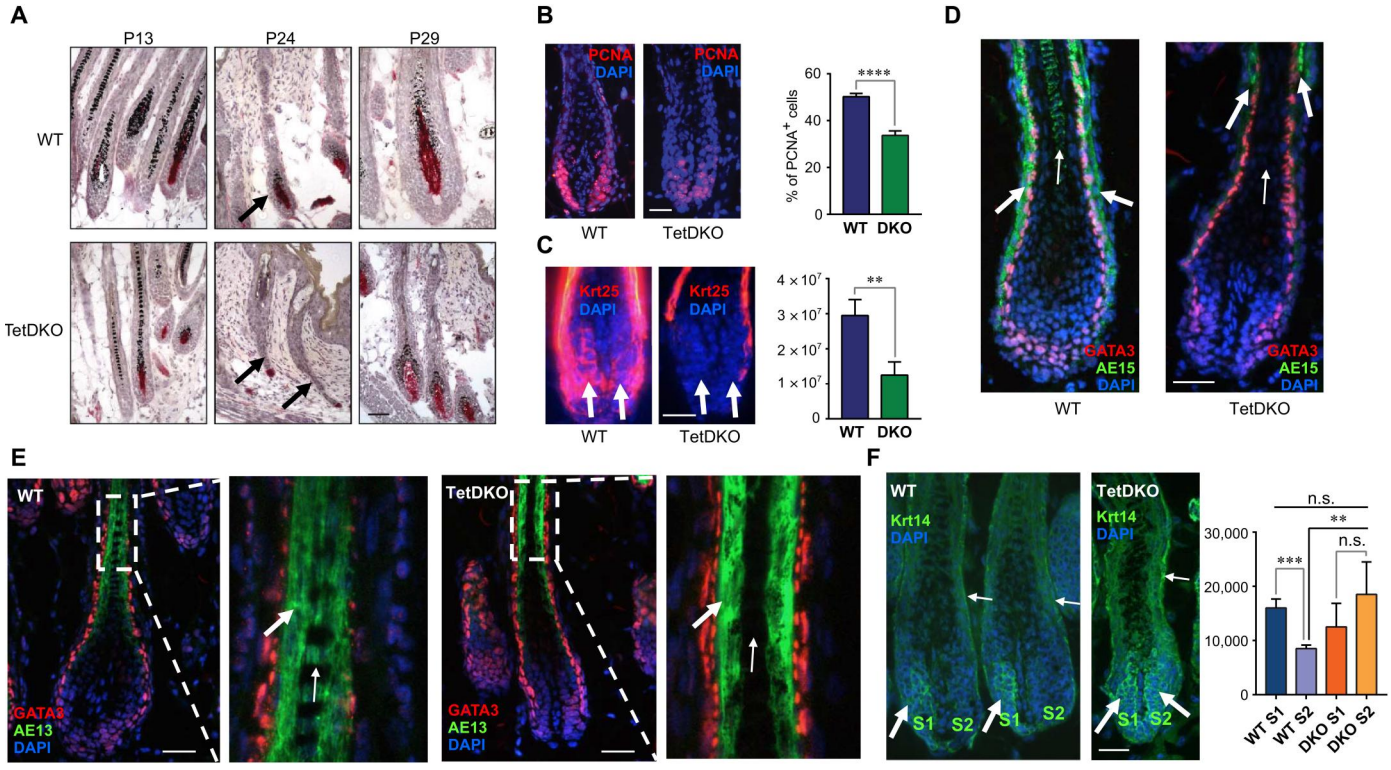

Fig. 3. Alterations in hair matrix keratinocyte proliferation and expression of terminal differentiation markers in TetDKO mice. (**A**) Alkaline phosphatase staining of WT and TetDKO HFs at P13, P24, and P29. At P24, early anagen follicles are seen in WT skin, while late catagen HFs are present in TetDKO mice (arrows), suggesting the delay in catagen-telogen-anagen transition. (**B**) Immunofluorescence staining for PCNA (red). Significant decrease of % of PCNA$^+$ cells in the hair matrix of TetDKO mice compared to controls. (**C**) Expression of the IRS-specific Krt25 is significantly ($P < 0.01$) decreased in the hair matrix keratinocytes of TetDKO mice compared to WT controls (arrows). *Y* value, relative fluorescence level. (**D**) Expression of the trichohyalin depicted by AE15 antibody (green) is markedly decreased in the HF IRS (large arrows) visualized by anti-GATA3 antibody (red) and hair shaft (small arrows) of TetDKO mice compared to WT controls. (**E**) Hair keratin expression depicted by AE13 antibody (green) is decreased in the hair medulla of TetDKO mice (small arrows). Strong AE13 immunofluorescence is seen in the hair cortex (large arrows) and medulla (small arrow) of the HF in WT mice. (**F**) Krt14 (green) is expressed in the HF outer root sheath in WT and TetDKO mice (small arrows) and unilaterally (S1) in the WT hair matrix keratinocytes. In TetDKO mice, Krt14 expression is seen on both sides (S1 and S2) of the hair matrix. Significant increase ($P < 0.01$) of the S2-Krt14 expression is seen in TetDKO mice compared to WT controls. *Y* value, relative fluorescence level. Cell nuclei are counterstained by DAPI (B to F). Data are presented as means ± SD. $^{**}P \leq 0.01$; $^{***}P \leq 0.001$; $^{****}P \leq 0.0001$; Student's *t* test. Scale bars, 25 (A) and 50 μm (D to F).

Tet2/Tet3 deficiency is accompanied by global changes in the DNA methylation, chromatin accessibility, and transcription factor binding

To assess changes in a global genome methylation status upon *Tet2/3* ablation, whole-genome bisulfite sequencing (WGBS) was performed using DNA isolated from the FACS-sorted hair matrix keratinocytes from P4.5 WT and TetDKO mice. We found that *Tet2/3* deficiency was accompanied by appearance of 11,086 differentially methylated regions (DMRs) showing an increase of DNA methylation in the genome of hair matrix keratinocytes globally (Fig. 5A and table S2). Genes that constitute the Keratin type I and II loci and occupying the corresponding TADs on mouse chromosomes 11 and 15 (TAD 11-085 and 15-082, respectively) (*44*) also showed an increase of DNA methylation upon *Tet2/3* ablation (Fig. 5A).

Because an increase of DNA methylation at regulatory elements is associated with decrease of chromatin accessibility, while the gene body methylation correlates with active transcription (*45*), we correlated the WGBS data with Assay for Transposase-Accessible Chromatin with high-throughput sequencing (ATAC-seq) data and found 1645 DMR (>40%) regions with decreased chromatin accessibility in TetDKO mice (Fig. 5B and fig. S5A). However, we also found an increase of chromatin accessibility in 3027 regions with increased DNA methylation upon *Tet2/Tet3* ablations (Fig. 5B). Similar changes were seen in the Keratin type I/II gene loci (Fig. 5B).

Although vast majority of the DMRs and regions exhibiting changes in the ATAC-seq status in TetDKO mice were associated with introns and intergenic regions, several hundreds of such regions showed associations with gene promoters (DMRs: 298; ATAC-seq changed regions: 215) and enhancers (375 and 263, respectively) globally (Fig. 5B). Associations between the DMRs, regions with changed chromatin accessibility, gene promoters and enhancers were also seen in the Keratin type I/II gene loci (Fig. 5B). Further analyses showed an increase of the DNA methylation within the regions containing the repressed ATAC-seq peaks, while only relatively minor changes in the DNA methylation status were seen among the ATAC-seq peaks increased or unchanged upon the *Tet2/Tet3* ablation (Fig. 5C and fig. S5, B and C).

Next, we performed the motif analyses of the genomic regions with significantly reduced chromatin accessibility in the TetDKO mice and found the enrichments of the binding sites for Dlx3 and

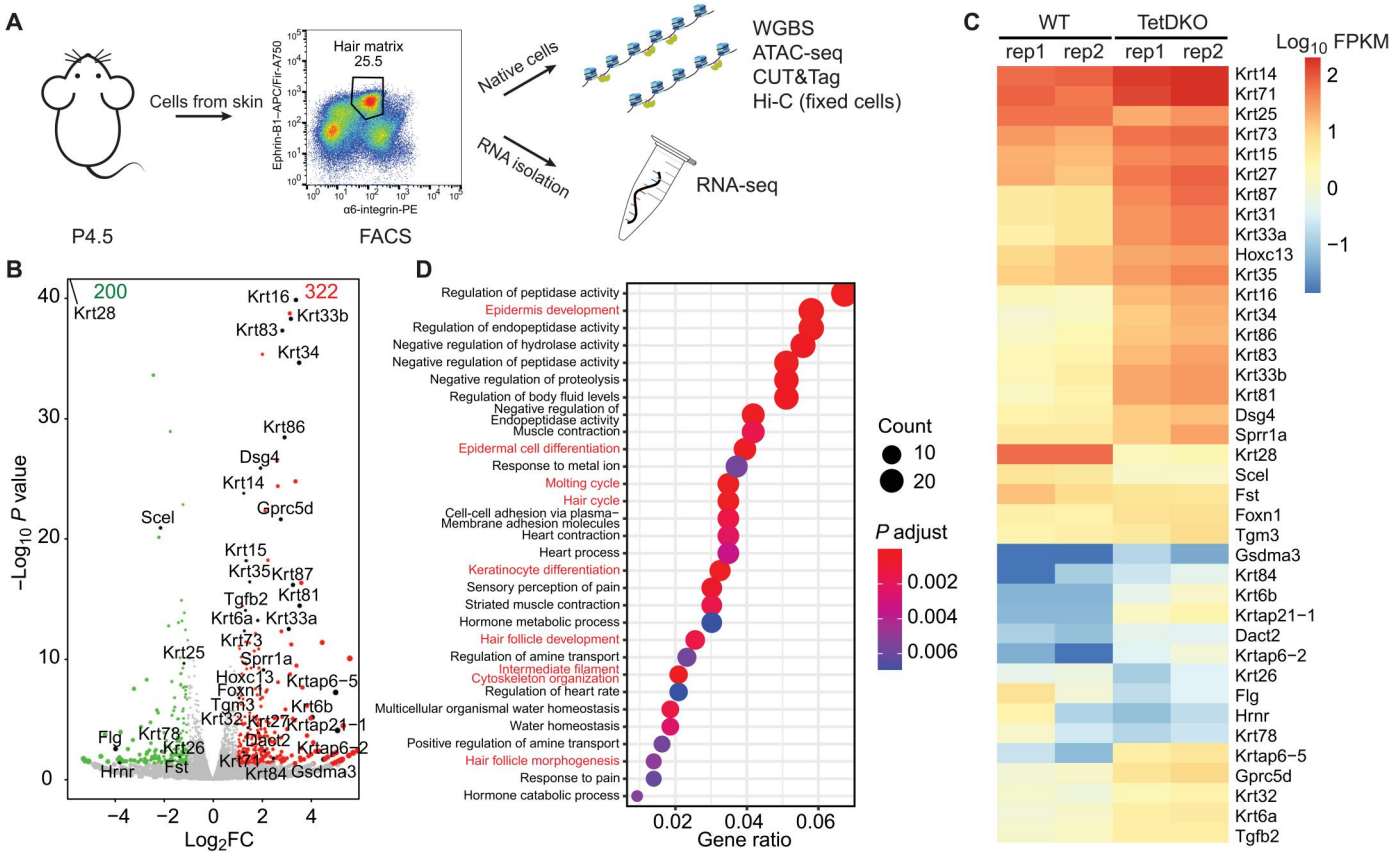

Fig. 4. Alterations of gene expression in hair matrix keratinocytes of TetDKO mice. (**A**) Ephrin-B1–expressing population of hair matrix keratinocytes are sorted from dorsal skin of WT and TetDKO mice at P4.5. Workflow of the RNA-seq, CUT&Tag, and other deep sequencing assays. (**B**) Volcano plot is obtained from the RNA-seq data of WT and Tet DKO hair matrix keratinocytes. Two hundred genes are down-regulated (green) and 322 genes are up-regulated (red) in TetDKO mice compared to WT controls. Significantly changed genes related to skin development including HF are indicated. Cutoff: abs(log_2FC) ≥ 1 and $P \leq 0.05$. (**C**) Heatmap of significantly changed genes related to skin development/differentiation/hair growth in TetDKO mice compared to WT mice. (**D**) Gene ontology (GO) enrichment analysis of all significantly changed genes in TetDKO versus WT mice. Top 30 significantly enriched GO terms are shown with gene ratio, count, and adjusted *P* values.

Lhx2 transcription factors (Fig. 5D). The motif analyses of the ATAC-seq peaks that were increased in TetDKO mice as well as of the Pol2Ser5 peaks decreased in hair matrix keratinocytes of TetDKO mice also showed the enrichment for the Dlx3 motifs (fig. S5, D and E). In contrast to Dlx3 motifs, Lef1 motifs only showed enrichment among the ATAC-seq increased peaks in TetDKO mice (fig. S5D).

Dlx3 and Lef1 transcription factors are crucial regulators of hair matrix keratinocyte differentiation and hair keratin gene expression (*46*, *47*), while Lhx2 is also expressed in hair matrix keratinocytes (fig. S1E) (*48*). Despite the fact that the *Dlx3* and *Lef1* transcript levels and proteins were not affected by the *Tet2/Tet3* ablation (fig. S5F), hair matrix keratinocytes of TetDKO mice showed predominance of the regions with decreased 5hmC content and Dlx3 binding (240 and 686, respectively) over the regions with increased 5hmC and Dlx3 binding (12 and 124, respectively) (fig. S5G). However, a number of the Pol2Ser5 and Lef1 peaks that show increase in TetDKO mice (4606 and 1238, respectively) was higher than the number of the corresponding regions with the decreased Pol2Ser5 and Lef1 binding (207 and 406, respectively).

Majority of the Dlx3 and Lef1 peaks at the DMRs and the regions exhibiting changes in the ATAC-seq status in TetDKO mice were associated with the introns and intergenic regions, as well as with gene promoters and enhancers (fig. S5H). Global analyses of the Dlx3- and Lef1-enriched peaks revealed more than 1700 overlapped Dlx3/Lef1 peaks in hair matrix keratinocytes of WT and TetDKO (fig. S5I). Using the Homer findMotifs tool, we identified Dlx3 motifs within the Lef1-enriched peaks and Lef1 motifs within the Dlx3-enriched peaks in both WT and TetDKO samples. Dlx3 binding to gene promoters and enhancers decreased in TetDKO mice, while Lef1 binding is increased in both promoter and enhancer regions (fig. S5J). These data suggested the links between DNA methylation and chromatin accessibility at gene promoters and enhancers for Dlx3 and Lef1 transcription factors and suggest their distinct yet partially overlapping roles in the regulation of gene expression in hair matrix keratinocytes.

Hypermethylation of the *Krt25* and *Krt28* gene promoters upon *Tet2/3* deficiency is accompanied by decreased chromatin accessibility and Dlx3 binding

Because hair phenotype in TetDKO and TetTKO mice resembled the wooly hair syndrome in humans associated with mutations in the *Krt25* gene and characterized by the appearance of short, curly hairs in affected individuals (*42*), we focused further analyses

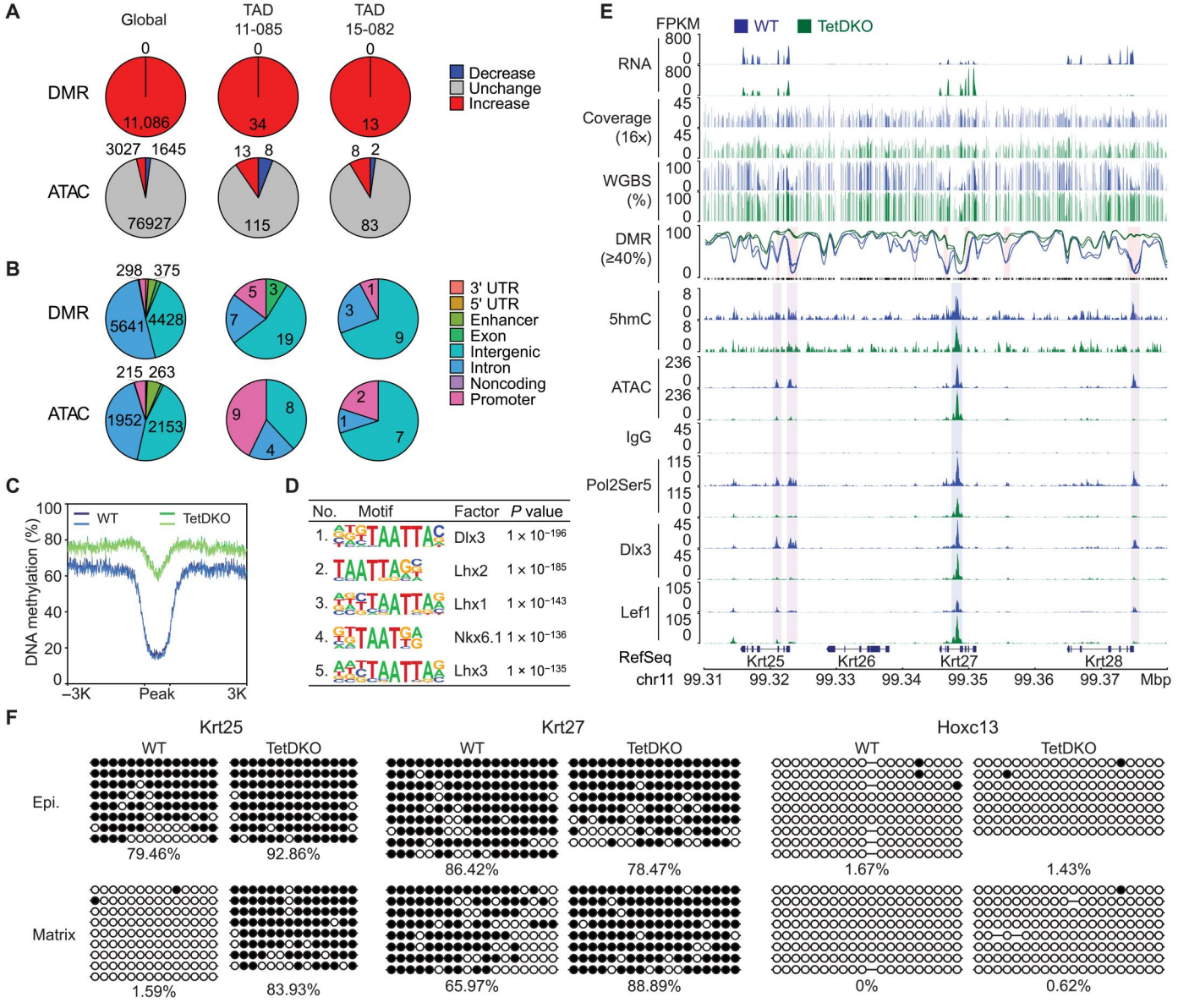

Fig. 5. Integrated analysis of DNA methylation, chromatin accessibility, and transcription factor binding sites in hair matrix keratinocytes upon *Tet2/3* ablation. (**A**) Pie plots of the WGBS DMRs, ATAC-seq peaks, and their distribution among different genomic regions in the whole-genome or within Keratin type I and II gene loci (TAD 11-085 and TAD 15-082, respectively) in the TetDKO in comparison to the control mice. DMR cutoff: abs(DMR) ≥ 40%; ATAC-seq cutoff: abs($\log_2$FC) ≥ 1 and $P \leq 0.05$. 3′UTR, 3′ untranslated region. (**B**) Distribution of DMRs and the increased or decreased regions of the chromatin accessibility in the TetDKO in comparison to the control mice in the indicated genomic elements. (**C**) Increase of DNA methylation in the regions with significantly repressed ATAC-seq peaks in TetDKO mice (replicate 1, green; replicate 2, light green) compared to WT mice (replicate 1, blue; replicate 2, light blue). (**D**) Motif analyses of the significantly reduced regions of chromatin accessibility in the TetDKO mice in comparison to the controls show enrichments for Dlx3 and Lhx2 transcription factor binding sites. (**E**) Tracks of the RNA-seq, WGBS, ATAC-seq, and CUT&Tag assays in the region of the Keratin type I locus of hair matrix keratinocytes harboring *Krt25* and *Krt28* genes (blue, WT mice; green, TetDKO mice). DMRs (absolute changes of DNA methylation, ≥40%), ATAC-seq, Dlx3, and Lef1 peaks are highlighted. *Y* axis values: (RNA-seq: FPKM; ATAC-seq, IgG, Pol2Ser5, Dlx3, and Lef1: coverage count; methylation and DMR: percentage). (**F**) Region-specific bisulfite sequencing of the *Krt25*, *Krt27*, and *Hoxc13* gene promoter regions using DNA isolated from the TetDKO and control mouse epidermal and hair matrix keratinocytes. Black circles, methylated cytosine; blank circles, unmethylated cytosine.

on the *Krt25-Krt27-Krt28* gene cluster at the Keratin type I locus encoding the IRS-specific keratins (*25*). We correlated changes in the DNA methylation status at gene promoters in this cluster with ATAC-seq data documenting chromatin and gene promoter accessibility (Fig. 5E). Decreased transcription of *Krt25* and *Krt28* genes in TetDKO mice was found to be associated with increase of DNA methylation at the promoter regions of these genes and markedly reduced ATAC-seq signals/chromatin accessibility (Fig. 5E).

In contrast to *Krt25* and *Krt28*, transcription of the neighboring *Krt27* gene increased in TetDKO mice, while its promoter methylation status and ATAC-seq signals were not changed (Fig. 5E). In WT mice, region-specific bisulfite sequencing of hair matrix

keratinocytes showed demethylation of the *Krt25* promoter, which remained methylated in epidermal keratinocytes (Fig. 5F). Significant increase of the DNA methylation status at the *Krt25* promoter was seen in hair matrix keratinocytes of TetDKO mice, while lack of differences in the methylation status of the *Krt27* or *Hoxc13* gene promoters was seen between these two keratinocyte populations in both WT and TetDKO mice (Fig. 5F).

Krt25 gene promoter showed conservation of the Dlx3 binding sites among different species including mice and humans (fig. S5K). Correlation of the WGBS, ATAC-seq, RNA-seq, and CUT&TAG-seq data for Dlx3, Lef1, and Pol2Ser5 data revealed marked decrease of the Dlx3 and Pol2Ser5 presence at the *Krt25* and *Krt28* gene promoters in hair matrix keratinocytes of TetDKO mice (Fig. 5E). Lef1 binding to *Krt28* gene promoter (but not to *Krt25* promoter) also decreased in TetDKO mice, while Lef1 binding to *Krt27* promoter increased and associated with the increase of Pol2Ser5 binding and gene transcription (Fig. 5E). These data suggest a possibility that *Krt27* gene expression in hair matrix keratinocytes is controlled by Lef1 in a DNA methylation–independent manner.

Hi-C analyses reveal rewiring of the chromatin interaction networks within Keratin type I/II loci upon *Tet2/3* ablation

Because gene promoters frequently interact with their distal regulatory elements including enhancers, silencers, insulators, and locus control regions in a three-dimensional nuclear space, we performed Hi-C chromosome conformation capture analyses to define the spatial chromatin interaction networks within the Keratin type I and II gene loci, as well as within the corresponding TADs on mouse chromosomes 11 and 15, respectively. We compared Hi-C data generated from the FACS-sorted hair matrix keratinocytes of WT and TetDKO mice and correlated with CUT&Tag-seq data for CCCTC-binding factor (CTCF), H3K27ac/H3K4me1 peaks for active enhancers, and with H3K27me3 peaks for Polycomb-dependent gene silencing (Fig. 6 and figs. S6, A to C, and S7). FACS-sorted basal epidermal keratinocytes of WT mice were used as controls of specificity of the Hi-C interactions depicted in hair matrix keratinocytes.

In WT mice, Hi-C chromatin interaction network within TAD 11-085 harboring Keratin type I locus depicted at a 5-kb resolution included 12 loops linking (i) gene promoters and intergenic regions/introns (8 loops), (ii) gene promoters and enhancers (3 loops), and (iii) two different intergenic regions (1 loop) (Fig. 6A and table S4). Within TAD 15-082 harboring Keratin type II locus, 19 chromatin loops included interactions between (i) enhancers and intergenic regions (9 loops), (ii) two different intergenic regions (8 loops), and (iii) the introns and intergenic regions (2 loops) (fig. S6 and table S4). In both TADs, chromatin interaction networks included only spatial contacts within the domains, while no contacts with neighboring TADs were seen across the TAD borders (Fig. 6A, fig. S6, and table S4). Comparative analyses of the Hi-C interactions between hair matrix and basal epidermal keratinocytes of WT mice revealed the presence of 5 and 6 common interactions, as well as 7 and 13 unique chromatin interactions in the Keratin type I and II loci, respectively (table S4).

However, a substantial rewiring of the chromatin interaction networks within both TADs was seen in TetDKO mice. Hi-C analyses revealed 13 newly formed chromatin interactions within TAD 11-085, while one of such interactions linked an intron of the *Ccr7* gene with intergenic region of the neighboring TAD 11-084 (Fig. 6A and table S4). Within TAD 15-082, seven new chromatin interactions were detected, including interactions between enhancers and intergenic regions (four chromatin interactions), as well as between different intergenic regions (three chromatin interactions) (fig. S6 and table S4).

In WT mice, Hi-C analyses of the Keratin type I locus revealed interactions between *Krt28* promoter and active enhancer located in the intergenic region between *Krt20* and *Krt23* genes (loop L1), which, in turn, interacted with two enhancers located at the central part of the TAD (loop L2) and closely to the TAD border (loop L4) (Fig. 6, A to C). Most likely, these interactions were anchored by CTCF, whose peaks were present at the *Krt28* gene promoter, as well as within the corresponding enhancers (Fig. 6, A, D, and E).

However, in TetDKO mice, increase of the *Krt28* promoter methylation was accompanied by a decrease of the CTCF occupancy at the promoter region and a shift of the corresponding chromatin loop (L1) by about 70 kb to a region outside of the *Krt28* promoter (Fig. 6, C and D). In addition, *Tet2/Tet3* ablation was accompanied by the disappearance of the loop L2 linking an enhancer located between the *Krt20* and *Krt23* genes with enhancer at the central part of the TAD as well as by the appearance of two newly formed loops linking the regulatory region of the *Krt14* gene with two enhancers located between the *Krt20* and *Krt23* genes (loop L3) and at the TAD flanking region (loop L5) (Fig. 6, A, C, and E, and fig. S7B).

The rewiring of spatial chromatin contacts including a significant reduction in the frequency of enhancer-promoter interactions for *Krt28* gene and appearance of additional enhancer-promoter contacts for *Krt14* gene suggest that such interactions may contribute to up-regulation of Krt14 gene and protein expressions in hair matrix keratinocytes of TetDKO mice (Figs. 3F and 4, B and C). Correlation of the Hi-C and ATAC-seq data revealed an increased chromatin accessibility of the *Krt14* gene regulatory region associated with increase of the Lef1 binding in TetDKO mice (Fig. 6E and fig. S7B). However, appearance of new chromatin loops within Keratin type I locus in TetDKO mice was not accompanied by changes in the DNA methylation status of gene promoters, CTCF binding, or Polycomb-dependent H3K27me3 occupancy (Fig. 6, A, D, and E, and fig. S7, A and B), thus suggesting that the effects of Tet2/Tet3 on new chromatin loop formation are probably DNA methylation and Polycomb independent.

In contrast to Keratin type I locus, comparison of the Hi-C data between WT and *Tet2/Tet3*-deficient mice revealed less extensive rewiring of the chromatin interaction network in the Keratin type II locus and corresponding TAD 15-082 (figs. S6 and S7C). *Tet2/Tet3* ablation was accompanied by appearance of newly formed chromatin loop in the vicinity of *Krt84* gene up-regulated in TetDKO mice, which link this region to the enhancer located in the central part of the TAD between the *Krt74* and *Krt72* genes (fig. S6, A to C). However, increase of expression of other keratin genes in the Keratin type II locus, such as *Krt6a/6b*, *Krt71*, *Krt73*, *Krt81*, *Krt83*, *Krt86*, and *Krt87*, in TetDKO mice was not associated with changes in the chromatin interaction networks in the locus, thus suggesting that other mechanisms are involved in the control of their expression.

Unexpectedly, in TetDKO mice, we also found an increase of Lef1 binding and chromatin accessibility at several genes encoding other hair-specific keratins and some epidermal keratins, such as

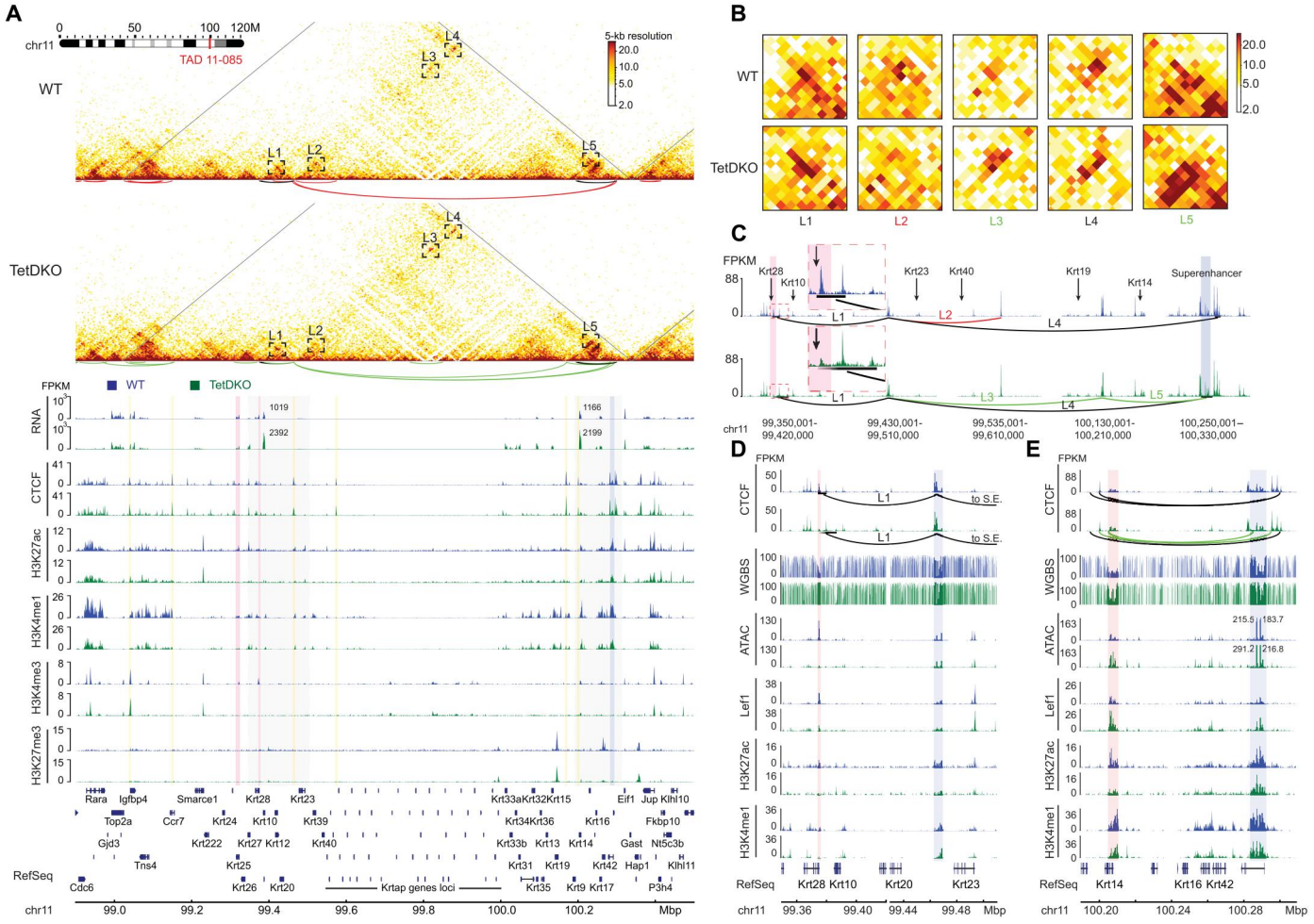

Fig. 6. Hi-C and CUT&Tag assay profiles in the Keratin type I locus and corresponding TAD 11-085. (**A**) Heatmap of the Hi-C chromatin interactions correlated with tracks of CTCF, H3K27ac, H3K4me1, H3K4me3, and H3K27me3 within TAD 11-085 and neighboring regions in hair matrix keratinocytes of WT (blue) and TetDKO (green) mice. Hi-C interactions: WT unique (red), TetDKO unique (green), and WT/TetDKO common (black). Dashed rectangles indicate unique and common Hi-C chromatin loops [L1 to L5; for details, see (B) and (C)] in the region between the *Krt25* and *Krt14* genes. Hi-C resolution: 5 kb. CUT&Tag *y* axis value: FPKM. CUT&Tag highlighted regions: *Krt25* and *Krt28* promoters (pink), CTCF anchors (yellow), and superenhancer region at the flanking part of the TAD (blue). (**B**) Details of the regions at the Hi-C heatmap showing chromatin loops L1 to L5 within Keratin type I locus in WT and TetDKO mice [see (A)]. (**C**) CTCF tracks and details of chromatin interaction loops L1 to L5. L1 loop insets: In TetDKO mice, CTCF peak disappears at the *Krt28* promoter, while left anchor of the L1 loop is shifted from the *Krt28* promoter to the neighboring intergenic region. L4 loop: Right anchor of the L4 loop is shifted to the *Krt14* regulatory region in TetDKO mice compared to WT controls. L3 and L5 loops: Newly formed chromatin interaction loops (L3 and L5) are seen in TetDKO mice. L5 links superenhancer located at the flanking part of Keratin type I locus to the *Krt14* regulatory region in TetDKO mice. (**D**) WGBS, ATAC-seq, and CUT&Tag track details for the L1 loop region. Highlighted regions: *Krt28* promoter (pink) and enhancer located between the *Krt20* and *Krt23* genes (blue). (**E**) WGBS, ATAC-seq, and CUT&Tag track details for the L3 to L5 loop region harboring *Krt14* and superenhancer (S.E.). Highlighted regions: *Krt14* promoter (pink) and superenhancer (blue).

Krt14, as well as at the superenhancer located in the flanking region of the Keratin type I locus (Fig. 6E and fig. S7B). Because chromatin accessibility at the regions with enhanced Lef1 binding was also increased (Fig. 6E and fig. S7B), these data suggest a DNA methylation–independent regulatory mechanism for these genes within Keratin type I locus.

5-Aza-2′-deoxycytidine treatment reverses the effects of *Tet2/3* ablation on *Krt25* and *Krt28* gene expression in hair matrix keratinocytes

To test whether the methylation status of the promoters and expressions of the *Krt25* and *Krt28* genes in TetDKO mice can be restored, we used DNA methylation inhibitor 5-aza-2′-deoxycytidine (5-aza) to treat TetDKO mice. 5-aza was injected subcutaneously at P2.5, and hair matrix keratinocytes were harvested, FACS-sorted at P4.5, and processed for RNA-seq, ATAC-seq, and CUT&Tag assays (Fig. 7A).

As expected, 5-aza treatment resulted in a marked decrease of the 5-mC and 5hmC immunofluorescence in the epidermis of WT mice (Fig. 7B). Globally, 5-aza treatment resulted in changes of the Pol2Ser5 occupancy in hair matrix keratinocytes—1117 regions showed decreased and 475 regions exhibited increased Pol2Ser5 occupancy in TetDKO mice after treatment compared to 5-aza–treated WT mice (fig. S8A). In TetDKO mice treated with 5-aza,

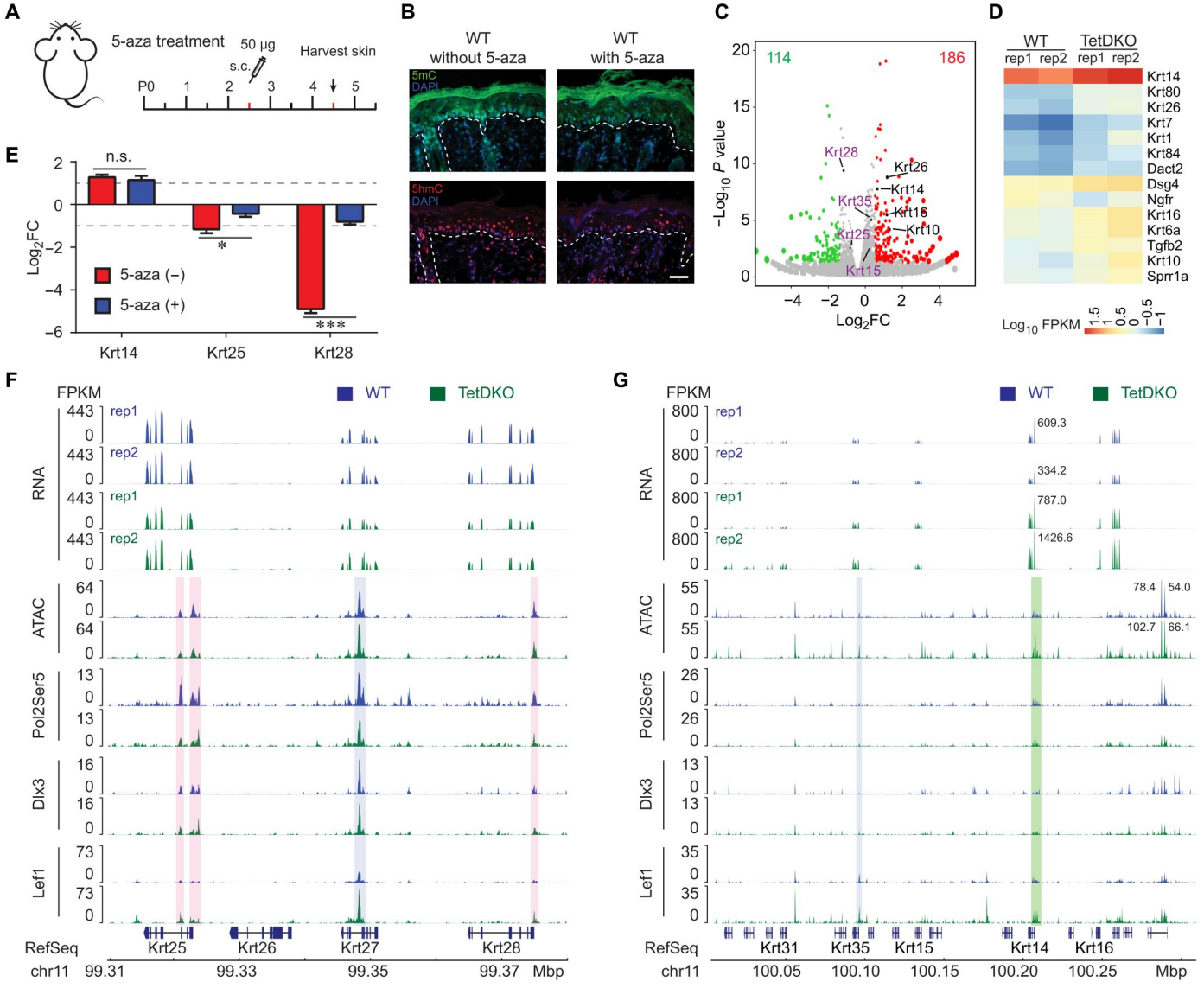

Fig. 7. Gene expression, chromatin accessibility and transcription factor binding analysis after 5-aza treatment in hair matrix keratinocytes of WT and TetDKO mice. (**A**) Scheme of the experiment with 5-aza treatment. sc., subcutaneous. (**B**) Immunofluorescence staining for 5mC (green) and 5hmC (red) in the skin with and without 5-aza treatment. Scale bar, 25 μm. (**C**) Volcano plot obtained from RNA-seq analyses of hair matrix keratinocytes of WT and TetDKO mice after 5-aza treatment. Down-regulated (green) and up-regulated (red) genes are highlighted. Significantly changed genes related to the skin and HF development are labeled (black). Cutoff: abs(log_2FC) ≥ 1 and $P \leq 0.05$. (**D**) Heatmap of significantly changed genes related to the skin and HF development after 5-aza treatment. (**E**) Expression levels of the *Krt14*, *Krt25*, and *Krt28* genes in hair matrix keratinocytes of TetDKO mice treated by control or 5-aza. Data are presented as means ± SD. *$P < 0.05$, ***$P \leq 0.001$; Student's *t* test. (**F** and **G**) Tracks of the RNA-seq, ATAC-seq, and CUT&Tag assay data in the region of the Keratin type I locus harboring hair and epidermal keratin genes in hair matrix keratinocytes of WT and TetDKO mice after 5-aza treatment. Promoters of *Krt25* and *Krt28* are highlighted with pink color, while *Krt27* gene is highlighted with blue color (F). Promoters of *Krt35* and *Krt14* genes are highlighted with blue and green colors, respectively (G).

RNA-seq analyses of hair matrix keratinocytes revealed changes in expression of 302 genes (186 genes up-regulated and 114 genes down-regulated) compared to the 5-aza–treated WT mice (Fig. 7, C and D, and fig. S8B).

Among the genes down-regulated in hair matrix keratinocytes and showing >25% increase of DNA methylation at their regulatory regions upon *Tet2/Tet3* ablation (Fig. 4B and table S1), we found 36 genes whose expression was significantly increased in TetDKO mice after 5-aza treatment (table S5). These genes encoded cell adhesion molecules and associated receptors (*Adgrf4* and *Dscaml1*), growth factor receptors and signaling components (*Map3k15*, *P2rx7*, *Ptpro*, and *Scube2*), metabolic and proteolytic enzymes (*Adh6b*, *Chst8*, *Dio2*, *Klk11*, *Padi4*, *Pipox*, *St8sia2*, and *Trib2*), components of the cytoskeleton/HF keratins (*Krt25* and *Krt28*), and regulators of transcription and nucleosome assembly (*Hist1h2ac*, *Hist1h2bn*, and *Stat5a*) (table S5).

At the levels of Keratin type I/II loci, 5-aza treatment of TetDKO mice caused distinct changes in gene expression, which can be grouped into three categories depending on their response to 5-aza: (i) genes up-regulated after 5-aza treatment (*Krt7*, *Krt17*,

Krt25, *Krt26*, *Krt28*, *Krt36*, *Krt42*, *Krt75*, and *Krt90*), (ii) genes down-regulated after 5-aza treatment (*Krt1*, *Krt6b*, *Krt10*, *Krt15*, *Krt16*, *Krt27*, *Krt31*, *Krt32*, *Krt33a*, *Krt33b*, *Krt77*, *Krt81*, *Krt83*, *Krt86*, and *Krt87),* and (iii) genes which expression remaining unchanged (29 genes) (fig. S8, C and D).

Genes up-regulated in TetDKO mice after 5-aza treatment included *Krt25* and *Krt28*: Similar to untreated mice, *Krt25* and *Krt28* were down-regulated in hair matrix keratinocytes of the control group of TetDKO mice compared to WT control group (Fig. 7E). However, the transcript levels of the *Krt25* and *Krt28* significantly increased in TetDKO mice after 5-aza treatment, almost reaching the expression levels of these genes seen in the 5-aza–treated WT mice (Fig. 7E). Increase of *Krt25* and *Krt28* expressions in TetDKO mice after 5-aza treatment was accompanied by an increase of the Dlx3 DNA binding affinity and chromatin accessibility to *Krt25* and *Krt28* promoters to the level seen in WT controls (Fig. 7F). DNA binding of the Lef1 to the *Krt25* and *Krt28* gene promoters was also increased in TetDKO mice after 5-aza treatment compared to WT controls (Fig. 7F).

Group of genes down-regulated in TetDKO mice after 5-aza treatment included many genes whose expression levels were higher in untreated TetDKO versus WT mice (Figs. 4, B and C, and 7, C and D). Unexpectedly, 5-aza–induced down-regulation of some of these genes (*Krt27* and *Krt35*) in TetDKO mice was also associated with increase of the Lef1 occupancy at their promoters (Fig. 7, F and G). These data suggested a complex effect of Lef1 on the expression of keratin genes, possibly dependent on the Lef1 interaction partners at the gene regulatory machinery stimulating or inhibiting gene transcription.

Last, a group of genes showing a resistance in their expression to the 5-aza treatment included *Krt14*, which transcript levels remained higher in TetDKO mice compared to WT mice treated by 5-aza (Fig. 7E). Similar to untreated TetDKO mice, the chromatin accessibility and Lef1 binding to *Krt14* promoter in TetDKO mice remained higher than in WT mice after 5-aza treatment (Fig. 7G). Thus, these data confirmed that, in contrast to *Krt25* and *Krt28* genes, the effects of *Tet2/Tet3* ablation on the expression of *Krt14* gene were most likely DNA methylation independent.

DISCUSSION

Execution of lineage-specific differentiation program in multipotent progenitor cells requires a high degree of coordination between the distinct levels of chromatin organization, and different classes of epigenetic regulators operate in concert to achieve a proper effect on DNA methylation and chromatin states during gene activation or silencing in differentiating cells (*2*, *4*, *6*, *16*, *20*, *49*). Here, we demonstrate that, at the levels of lineage-specific gene loci occupying individual TADs in the genome, Tet enzymes regulate execution of hair-specific differentiation program via at least three distinct mechanisms:

1) DNA methylation–dependent control of chromatin accessibility and Dlx3 binding and promoter activity of the *Krt25* and *Krt28* genes regulating hair shape;

2) DNA methylation–dependent regulation of interactions between the *Krt28* gene promoter and enhancer localized in the intergenic region of the corresponding TAD;

3) DNA methylation–independent rewiring of the chromatin interaction networks within TADs harboring Keratin type I and II gene loci occurring upon *Tet2/Tet3* deficiency and resulting in alterations of hair-specific gene expression program.

Our data reveal a list of genes whose DNA methylation status of regulatory regions and gene expression change can be explained by Tet-mediated DNA demethylation (Fig. 8). Group of these genes include *Krt25* and *Krt28*, and we show here that *Tet2/3* regulate DNA methylation status of the *Krt25* and *Krt28* promoters and their accessibility for Dlx3 transcription factor (Fig. 4). Hair phenotype seen in TetDKO mice is quite consistent with the data showing that mutation in the *KRT25* gene is associated with the wooly hair syndrome and appearance of short, curly hairs in affected human individuals (*42*). Mutations of the *Krt25* gene in mice also result in a wavy coat phenotype (*50*). Dlx3 transcription factor play key roles in the control of IRS-specific keratinocyte differentiation, regulation of hair shape, and directly controls expression of *Krt25* (*46*, *51*), while heterozygous *DLX3* mutations are also associated with formation of kinky/curly, sparse hairs, and hair loss (*52*). Thus, our data demonstrate the essential roles for Tet2/3 in the control of Dlx3/Krt25/Krt28 axis in hair matrix keratinocytes via regulating gene promoter methylation and chromatin accessibility (Fig. 8).

However, there are a number of genes in hair matrix keratinocytes, whose changes in expression in TetDKO mice cannot be explained by the DNA methylation changes. One of these genes is *Krt27* located between *Krt25* and *Krt28* in a 60-kb region of the Keratin type I locus. *Krt27* is functionally related to *Krt25* and *Krt28*, while its mutation results in curly hair phenotype in mice (*50*). Our data demonstrate that, despite a strong functional

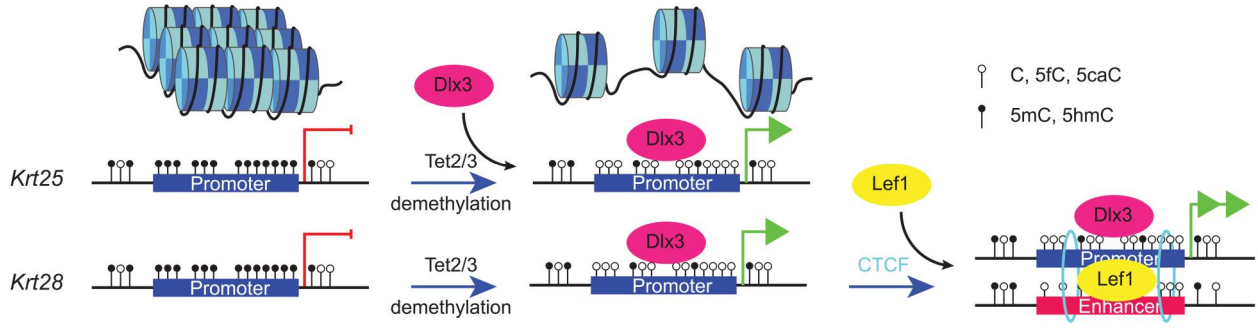

Fig. 8. Models for Tet2/3-dependent regulation of *Krt25* and *Krt28* genes in hair matrix keratinocytes. *Krt25* is activated by Tet2/3 through DNA demethylation, with increased chromatin accessibility and Dlx3 binding. *Krt28* is also activated by Tet2/3, which relies not only on the increase chromatin accessibility and Dlx3/Lef1 binding but also on CTCF-mediated promoter-enhancer interaction in a DNA methylation–dependent manner.

relevance to *Krt25* and *Krt28* genes, *Krt27* expression in hair matrix is regulated in DNA methylation–independent manner: In contrast to *Krt25* and *Krt28*, *Krt27* is up-regulated in TetDKO mice, while 5-aza treatment result in down-regulation of *Krt27* expression. These data suggest that transcription of the *Krt25*, *Krt27*, and *Krt28* genes is regulated quite differently, possibly via recruitment of the distinct sets of transcription factors for each gene promoter and/or via involvement of the distinct epigenetic mechanisms. However, these data are consistent with a current view on the catalytic activity–dependent and independent modes of Tet functions in the control of gene expression (*14*, *16*, *53*–*55*).

We demonstrate here that, in addition to direct effect on the *Krt25* and *Krt28* gene promoters, Tet2/3 regulate composition of the chromatin interaction networks within Keratin type I and II gene loci including enhancer-promoter interactions (Fig. 6). By using Hi-C analyses, we show a substantial rewiring of the chromatin interaction networks in these loci upon *Tet2/3* ablation including changes in the existing chromatin loops and formation of new loops linking gene promoters and enhancers (Fig. 6 and table S4). However, we understand that captured Hi-C analyzes are required to generate a detailed high-resolution map of changes in the chromatin interaction networks within Keratin type I/II gene loci upon *Tet2/Tet3* ablation, as well as the impact of the distinct chromatin interactions on gene expression needs to be validated in functional assays.

Changes in Hi-C chromatin interactions can be due the loss of 5hmC or increase of 5mC, while DNA demethylation (to unmodified C) and oxidation of 5mC to 5hmC may also play different roles. The effects of Tet2/3 on enhancer-promoter networks appears to be quite distinct: On one hand, Tet2/3-dependent demethylation of the *Krt28* promoter is associated with the binding of CTCF at the promoter region and interaction of the promoter with distal enhancer localized in the intergenic region of the corresponding TAD on chromosome 11 (Fig. 8). On the other hand, Tet2/3 might repress interactions of a number of keratin gene promoters including *Krt14* with superenhancer localized at the flanking region of Keratin type I locus, presumably via interaction with other regulators of gene expression and chromatin accessibility.

Catalytic activity–independent functions of *Tet* genes have been demonstrated in different models and contexts including embryonic and hematopoietic stem cells (*54*, *55*). Recent data demonstrate that noncatalytic activity of Tet1 is mediated via protein-protein interactions of Tet1 with Sin3a that promotes Ezh2 recruitment to the promoters of bivalent genes and their repression (*54*). Our data showing lack of changes in the histone H3K27me3 chromatin status within Keratin type I/II loci of hair matrix keratinocytes upon *Tet2/3* ablation suggest that Tet2/3 interactions with Polycomb group proteins in repressing gene transcription and/or enhancer activity are rather unlikely. Thus, additional analyses are required to fully uncover the Tet2/3 interaction network with distinct transcriptional repressors and/or chromatin regulators to inhibit expression of the genes (such as *Krt14* gene) normally down-regulated in hair matrix keratinocytes and markedly up-regulated upon *Tet2/3* gene ablation.

Our data also suggest distinct but yet overlapping roles for Dlx3 and Lef1 transcription factors in the control of keratin gene expression in hair matrix keratinocytes. There are more than 1700 overlapped Dlx3/Lef1-enriched peaks in hair matrix keratinocytes, while Dlx3 motifs are present within the Lef1-enriched peaks and vice versa. We show that the regions with decreased 5hmC content and Dlx3 binding predominate over the regions with increased 5hmC and Dlx3 binding in hair matrix keratinocytes of TetDKO mice (fig. S5G). However, in contrast to Dlx3, a number of the Pol2Ser5 and Lef1 binding regions increased in TetDKO mice, while enhanced Lef1 binding is associated with increase of chromatin accessibility at several genes encoding other hair-specific keratins (for example, *Krt27*) and some epidermal keratins, such as *Krt14* (Fig. 6E and fig. S7B). These data are consistent with a recent report demonstrating a role for Lef1 in the formation and maintenance of open chromatin structure in T cells (*56*) and suggest a similar role for Lef1 in regulation of chromatin accessibility and expression of hair keratin genes.

However, additional analyses are required to check whether Dlx3 also play a role in the control of chromatin remodeling in hair matrix keratinocytes via interaction with distinct components of epigenetic machinery or via direct control of their expression, a function demonstrated previously for p63 transcription factor (*20*, *49*). Furthermore, it is still unclear whether Tet2/Tet3 are capable of interacting with Lef1 and other transcription factors (such as Foxn1, Hoxc13, and Lhx2) at the promoters of the hair and epidermal keratin genes, and whether *Tet2/Tet3* ablation somehow promote their accessibility to gene promoters. Also, the potential role of *Tet* genes in the control of hair cycle–associated changes of the DNA methylation status in epithelial stem cells during transition from the quiescent to active state (*26*) needs to be carefully investigated by using stem cell–specific Cre drivers for *Tet* gene ablation.

In conclusion, these data demonstrate an essential role for *Tet2/3* in the control of hair keratin gene expression, enhancer-promoter interactions, and three-dimensional chromatin organization in lineage-specific gene loci required for hair shaft formation. Translation of these data to human skin and analyses of the roles of Tet-dependent DNA demethylation in the control of human hair growth and potential contribution of TET proteins to pathogenesis of hair growth abnormalities including different forms of hair loss may promote development on novel therapeutic interventions based on modulation of DNA methylation dynamics in the HF and skin.

MATERIALS AND METHODS

Mice and tissue collection

Mice were kept and breeding in Animal Science Center of Boston University under the conditions of 12/12-hour light/dark cycles, a temperature of ~22°C, and humidity of ~50%, following the protocols and approval of Institutional Animal Care and Use Committee. *Tet2* floxed/floxed (fl/fl) mice (*37*) were obtained from The Jackson Laboratory, and *Tet3* fl/fl mice were obtained from W. Reik (Babraham Institute, Cambridge, UK) (*38*). *Tet1* fl/fl, *Tet2* fl/fl, and *Tet3* fl/fl mice were generated in G.-L.X.'s laboratory (*39*). *Krt14-Cre* mice were obtained from The Jackson Laboratory (stock no. 018964) and used to simultaneously ablate *Tet2* and *Tet3* genes (TetDKO mice) or all three *Tet* genes (TetTKO mice) in keratinocytes. Genotyping of mice was performed using polymerase chain reaction (PCR), as recommended by the supplier. Skin samples were collected from mice at distinct days of embryonic and postnatal development (E18.5 and P0.5 to P56), as described before (*57*).

Fluorescence-activated cell sorting

Whole back skin was isolated from mice at P4.5 and incubated with 0.5% of Dispase II (Roche, #45147700) at 4°C overnight in 1× Hanks′ balanced salt solution (Sigma-Aldrich, #H2387) without Ca^{2+} and Mg^{2+}. Epidermis and dermis were cut into small pieces and digested with Accutase (Gibco, #2310194) containing 0.1% of Liberase DH (Roche, #05401054001) at 37°C and centrifuged at 800 rpm for 20 min. Cells were filtered with a 70-μm nylon mesh and stained with CD140a-Allophycocyanin (APC) (1:150; Invitrogen, #2213095), CD31-APC (1:150; Invitrogen, #219898), CD207-APC (1:150; BioLegend, #B301300), CD117-APC (1:150; Invitrogen, #2162256), α6-integrin-Phycoerythrin (PE) (1:500; Invitrogen, #2196653), and Sca1-Fluorescein isothyocyanate (FITC) (1:300; eBioscience, #E00760-1633) antibodies for 30 min on ice and washed by using 1% fetal bovine serum (FBS), followed by staining with anti–Ephrin-B1 antibodies (1:25; R&D Systems, #BAF473), streptavidin-APC/fire–Alexa Fluor 750 (1:250; BioLegend, #405250), and LEAVE/DEAD Fixable Violet Dead Cell Stain Kit (1:1000; Life Technologies, #L34955) for 30 min on ice intercepted by 1% FBS washing between each staining. Hair matrix keratinocytes were separated from other skin cell populations based on their Ephrin-$B1^+$ staining (*43*).

Immunohistochemistry and immunohistomorphometry

Skin samples and embryos were embedded into Tissue-Tek optimal cutting temperature (O.C.T.) medium and stored at −80°C before cutting. For immunohistochemistry staining, 10-μm cryosections were fixed with 4% paraformaldehyde at room temperature for 10 min, and followed by the antigen retrieval procedure at pH 6.0 (95°C for 20 min). Sections were immunostained with primary antibody at 4°C overnight and secondary antibody at 37°C for 40 min. Last, the stained slides are embedded with 4′,6-diamidino-2-phenylindole (DAPI) medium. The following primary antibodies against corresponding antigens were used: Tet1 (1:100; ABclonal, #A1506), Tet2 (1:100; Millipore, #ABE364), Tet2 (1:100; Millipore, #MABE1132), Tet3 (1:150; ABclonal, #A13453), Tet3 (1:50; Active Motif, #61744), 5hmC (1:500; Active Motif, #39769), 5mC (1:200; EpiGentek, #A-1014), Ki67 (1:200; Abcam, #ab15580), Krt10 (1:500; BioLegend, #905401), Krt14 (1:1000; Covance, #142028001), Krt14-FITC (1:50; Covance, #142028001), Krt25 (1:200; LC Sciences, #lc-375059), loricrin (1:1000; Covance, #147332002), pan-cytokeratin AE13 Alexa Fluor 488 (1:100; Santa Cruz Biotechnology, #SC-57012), proliferating cell nuclear antigen (PCNA) (1:200; BioLegend, #307904), trichohyalin AE15 Alexa Fluor 488 (1:200; Santa Cruz Biotechnology, #SC-80607 AF488), GATA binding protein 3 (GATA3) (1:50; Santa Cruz Biotechnology, #sc-268), Lhx2 (1:200; Invitrogen, #PA5-78287), and Ephrin-B1 (1:50; R&D Systems, #SC-80607 AF488).

Alkaline phosphatase staining on 10-μm freshly cut cryosections was performed, as described previously (*58*). After phosphate-buffered saline washing, sections were counterstained with hematoxylin and embedded with glycerol gelatin.

For histomorphometry analysis, every 10th cryosection of dorsal skin from TetDKO, TetTKO, and WT mice was used to exclude the repetitive evaluation of the same HF. The epidermal thickness and the number of HFs per millimeter of epidermal length were calculated using sections from dorsal skin of TetDKO, TetTKO, and WT mice at P1.5 (n = 3 to 5 per each experimental group). Keratinocyte proliferation was assessed by the calculation of the percentage of $PCNA^+$ cells in the hair matrix and by quantification of $Ki67^+$ cells per hair bulb in 40 to 60 HFs of WT (n = 3 to 5) and TetDKO mice (n = 3 to 5) at P4.5 to P11.5. The hair bulb diameter was measured across the widest part of the bulb (Auber line). Together, HFs in 50 to 60 microscopic fields from distinct time points were analyzed and compared with a corresponding number of HF from the appropriate age-matched WT mice. Quantification of immunofluorescence intensity or CTCF was determined in 40 to 60 HFs of WT (n = 3 to 5) and TetDKO mice (n = 3 to 5) using ImageJ software, as described previously (*2*). Data were pooled, the means ± SD were calculated, and statistical analysis was performed using an unpaired Student′s t test.

For the assessment of the hair shaft length and width, hairs were plucked from the back skin of TetDKO, TetTKO, and WT mice (n + 4 to 5 per each mouse strain) in the telogen phase of the hair cycle (P20 to P23). Four hair types were distinguished in WT mice on the basis of their hair length, number of kinks, and medulla width (*41*). Hair shaft length and width of about 50 plucked hair shafts per animal were measured using ImageJ software (*2*). Data were pooled, the means ± SD were calculated, and statistical analysis was performed using an unpaired Student′s t test.

RNA sequencing

Total RNA was isolated from primary keratinocytes (1 million cells) with TRIzol Reagent (Thermo Fisher Scientific, #15596026) and eluted in 50 μl of deoxyribonuclease (DNase)/ ribonuclease (RNase)–free water. Total RNA was isolated from sorted hair matrix keratinocytes (100 to 200 thousand cells) with the RNeasy Micro Kit (QIAGEN, #74004) according to the manufacturer′s protocol and eluted in 12 μl of DNase/RNase-free water. Integrity of RNA was assessed on 2100 Bioanalyzer Instrument (Agilent Technologies Inc.), and only samples with RNA integrity number (RIN) factor above 7.5 were used for next-generation sequencing (NGS) library preparation. For RNA-seq, approximately 10 μg of the total RNA was used to remove ribosomal RNA according to the manuscript of the Epicentre Ribo-Zero Gold Kit (Illumina, San Diego, USA). Following purification, the ribo-minus RNA fractions is fragmented into small pieces using divalent cations under elevated temperature. Then, the cleaved RNA fragments were reverse-transcribed to create the final cDNA library in accordance with a strand-specific library preparation by deoxyUridine Triphosphate (dUTP) method. The Zymo-Seq RiboFree Total RNA Library Kit (Zymo, #R3000) was used for cDNA synthesis and stranded library preparation. The average insert size for the paired-end libraries was 300 ± 50 bp. The paired-end 2 × 150 bp sequencing was performed on an Illumina HiSeq 4000 platform.

Whole-genome bisulfite sequencing

Genomic DNA was isolated from 400,000 sorted native or formaldehyde fixed cells with lysis buffer [100 mM tris-HCl (pH 8.8), 5 mM EDTA, 200 mM NaCl, 0.2% SDS, and proteinase K (0.4 mg/ml)] at 55°C for 4 hours, sheared to the length of 300 to 500 bp, and eluted in 20 μl of double-distilled water (ddH_2O). DNA methylation conversion was performed with an EZ DNA Methylation-Gold kit (Zymo, #5005). Briefly, 20 μl of sheared genomic DNA was converted with 130 μl of the CT Conversion Reagent. The converted genomic DNA binds to Zymo-Spin IC Column and was proceeded for desulphonation with 200 μl of M-Desulphonation buffer and eluted in 17 μl of low Tris EDTA (TE) buffer. Bisulfite

sequencing DNA libraries were prepared by using the ACCEL-NGS Methyl-Seq DNA Library kit (Swift Biosciences, #30024 and #x6024) with 7 to 9 cycles′ PCR amplification, as the manual described. Paired-end sequencing was performed in the Illumina NovaSeq 6000 system (2 × 150 bp) for WGBS.

ATAC-seq

For the analyses of chromatin accessibility, an ATAC-seq kit (Active Motif, #81286) was used, as described previously (*59*). About 100,000 sorted cells were suspended in 100 μl of ice-cold ATAC lysis buffer for nuclei extraction, and nuclei were incubated in 50 μl of Tagmentation Master Mix for DNA tagmentation. After purification, the DNA was amplified with NEBNext High-Fidelity 2× PCR Master Mix [New England Biolabs (NEB), #M0541], as well as with unique i5 and i7 index primers for 10 cycles to prepare DNA library. Paired-end sequencing is performed in the Illumina NextSeq500 Midoutput PE75 System (2 × 75 bp).

CUT&Tag sequencing

CUT&Tag assay was carried out with the CUTANA CUT&Tag kit (EpiCypher) according to the manufacturer′s protocol. Briefly, nuclei of 100,000 sorted hair matrix keratinocytes were isolated with nuclear extraction buffer [20 mM Hepes-KOH (pH 7.9), 10 mM KCl, 0.1% Triton X-100, 20% glycerol, 0.5 mM spermidine, and 1× cOmplete Protease Inhibitor Cocktail] and attached to concanavalin A linked magnetic beads activated with bead activation buffer [20 mM Hepes-KOH (pH 7.9), 10 mM KCl, 1 mM $CaCl_2$, and 1 mM $MnCl_2$]. Beads with attaching nuclei were incubated with 0.5 μg of primary antibody in the Digitonin150 buffer [20 mM Hepes (pH 7.5), 150 mM NaCl, 0.5 mM spermidine, 0.01% digitonin, and 1× cOmplete Protease Inhibitor Cocktail] containing 2 mM EDTA at 4°C with gentle shaking for overnight and followed by incubation with 0.5 μg of secondary antibodies in Digitonin150 buffer at room temperature for 30 min. After washing twice with Digitonin150 buffer, beads were incubated with 2.5 μl of pAG-Tn5 in Wash300 Buffer [20 mM Hepes (pH 7.5), 300 mM NaCl, 0.5 mM spermidine, and 1× cOmplete Protease Inhibitor Cocktail] containing 0.01% digitonin at room temperature for 1 hour. Beads with attaching nuclei were washed with Wash300 buffer containing digitonin and incubated in Wash300 buffer containing 10 mM $MgCl_2$ at 37°C for 1 hour to perform chromatin tagmentation. Beads were washed with tris(hydroxymethyl)methylamino]propanesulfonic acid (TAPS) buffer [10 mM TAPS (pH 8.5) and 0.2 mM EDTA], and the DNA was released in 5 μl of SDS release buffer [10 mM TAPS (pH 8.5) and 0.1% SDS] at 55°C for 1 hour and quenched with 15 μl of 0.67% Triton X-100. DNA libraries were amplified for 18 to 21 cycles with 25 μl of NEBNext High-Fidelity 2× PCR Master Mix (NEB, #M0541) and 2.5 μl of unique i5 and i7 index primers for Illumina. Paired-end sequencing was performed in Illumina NextSeq2000 P2 PE50 system (2 × 50 bp). Antibodies used were against 5hmC (Active Motif, #39769), Dlx3 (Abcam, #ab66390), Lef1 (Cell Signaling, #2230), Pol2Ser5 (Abcam, #ab5408), CTCF (Diagenode, #C15410210), H3K4me1 (Diagenode, #C1541094), H3K4me3 (Abcam, #ab12209), H3K27ac (Abcam, #ab4729), and H3K27me3 (Millipore, #07-449).

Hi-C sequencing

Hi-C analyses were carried out with the Hi-C Kit (Arima Genomics, San Diego, CA) according to the manufacturer′s protocol. A 1.3 M sorted hair matrix keratinocytes obtained from 8 to 10 control and TetDKO mice at P4.5 were fixed with formaldehyde in a final concentration to 2% at room temperature for 10 min for DNA cross-linking and quenched with glycine in a final concentration to 300 mM and then suspended in 20 μl of lysis buffer. FACS-sorted basal epidermal keratinocytes of WT mice were used as controls of specificity of the Hi-C interactions depicted in hair matrix keratinocytes. Cross-linked DNA of the cells was digested with Arima rescriction enzyme (RE) cocktail. The ends of DNA fragments were repaired, then labeled with biotin, and religated again. Biotin-labeled DNA was sheared to 300 to 500 bp and enriched with enrichment beads. DNA libraries were prepared by using the Swift Biosciences Accel-NGS 2S Plus DNA Library Kit with a 5 to 7 cycles′ amplification. DNA libraries of the samples for paired-end sequencing were performed in the Illumina NovaSeq 6000 system (2 × 150 bp). Juicer platform (version 1.6) was used for generation of the Hi-C maps from Fastq raw data files, data analysis, and loop calling (*60*).

Statistics, data analyses, and reproducibility

Quantitative data were presented as means ± SD from at least two independent replicates except Hi-C and CUT&Tag sequencing assays. Statistically significant differences between different groups were compared with a two-way unpaired Student′s *t* test [$P \leq 0.05$ and absolute (fold change (FC) ≥ 1 if applicable]. TetDKO, TetTKO, and corresponding WT control mice were from the same litter (except samples used for Hi-C analyses), which was confirmed by genotyping. All samples were included during the analysis, and investigators were blinded to allocate or pick up samples during performing all assays.

All the programs and pipeline used in current project are open-access versions. Online resources are the following: MACS2 version 2.2.7 (https://github.com/macs3-project/MACS/releases), R x64 4.0.3 (https://cloud.r-project.org/), Bowtie2 version 2.4.2 (http://bowtie-bio.sourceforge.net/bowtie2/index.shtml), STAR version 2.7.9a (https://github.com/alexdobin/STAR), Hisat2 version 2.2.0 (http://daehwankimlab.github.io/hisat2), Bismark version 0.23.0 (www.bioinformatics.babraham.ac.uk/projects/bismark), Juicer version 1.6 (https://github.com/aidenlab/juicer/archive/1.6.tar.gz), Samtools version 1.10 (www.htslib.org), Bedtools version 2.30.0 (http://bedtools.readthedocs.io/en/latest/), deepTools version 3.5.1 (http://deeptools.readthedocs.io), HTSeq version 0.11.0 (http://htseq.readthedocs.io), Homer version 4.10 (http://homer.ucsd.edu/homer/index.html), pyGenomeTracks version 3.6 (https://github.com/deeptools/pyGenomeTracks), DEseq2 version 1.34.0 (https://bioconductor.org/packages/release/bioc/html/DESeq2.html), and DiffBind version 3.4.0 (https://bioconductor.org/packages/release/bioc/html/DiffBind.html).

Supplementary Materials

This PDF file includes:
Figs. S1 to S8

Other Supplementary Material for this manuscript includes the following:
Tables S1 to S5

View/request a protocol for this paper from *Bio-protocol*.

REFERENCES AND NOTES

1. C. Blanpain, E. Fuchs, Stem cell plasticity. Plasticity of epithelial stem cells in tissue regeneration. *Science* **344**, 1242281 (2014).
2. M. I. Ahmed, M. Alam, V. U. Emelianov, K. Poterlowicz, A. Patel, A. A. Sharov, A. N. Mardaryev, N. V. Botchkareva, MicroRNA-214 controls skin and hair follicle development by modulating the activity of the Wnt pathway. *J. Cell Biol.* **207**, 549–567 (2014).
3. R. C. Adam, E. Fuchs, The yin and yang of chromatin dynamics in stem cell fate selection. *Trends Genet.* **32**, 89–100 (2016).
4. A. Avgustinova, S. A. Benitah, Epigenetic control of adult stem cell function. *Nat. Rev. Mol. Cell Biol.* **17**, 643–658 (2016).
5. D. Gokbuget, R. Blelloch, Epigenetic control of transcriptional regulation in pluripotency and early differentiation. *Development* **146**, dev164772 (2019).
6. Y. A. Miroshnikova, I. Cohen, E. Ezhkova, S. A. Wickstrom, Epigenetic gene regulation, chromatin structure, and force-induced chromatin remodelling in epidermal development and homeostasis. *Curr. Opin. Genet. Dev.* **55**, 46–51 (2019).
7. P. Carninci, T. Kasukawa, S. Katayama, J. Gough, M. C. Frith, N. Maeda, R. Oyama, T. Ravasi, B. Lenhard, C. Wells, R. Kodzius, K. Shimokawa, V. B. Bajic, S. E. Brenner, S. Batalov, A. R. R. Forrest, M. Zavolan, M. J. Davis, L. G. Wilming, V. Aidinis, J. E. Allen, A. Ambesi-Impiombato, R. Apweiler, R. N. Aturaliya, T. L. Bailey, M. Bansal, L. Baxter, K. W. Beisel, T. Bersano, H. Bono, A. M. Chalk, K. P. Chiu, V. Choudhary, A. Christoffels, D. R. Clutterbuck, M. L. Crowe, E. Dalla, B. P. Dalrymple, B. de Bono, G. D. Gatta, D. di Bernardo, T. Down, P. Engstrom, M. Fagiolini, G. Faulkner, C. F. Fletcher, T. Fukushima, M. Furuno, S. Futaki, M. Gariboldi, P. Georgii-Hemming, T. R. Gingeras, T. Gojobori, R. E. Green, S. Gustincich, M. Harbers, Y. Hayashi, T. K. Hensch, N. Hirokawa, D. Hill, L. Huminiecki, M. Iacono, K. Ikeo, A. Iwama, T. Ishikawa, M. Jakt, A. Kanapin, M. Katoh, Y. Kawasawa, J. Kelso, H. Kitamura, H. Kitano, G. Kollias, S. P. T. Krishnan, A. Kruger, S. K. Kummerfeld, I. V. Kurochkin, L. F. Lareau, D. Lazarevic, L. Lipovich, J. Liu, S. Liuni, S. McWilliam, M. M. Babu, M. Madera, L. Marchionni, H. Matsuda, S. Matsuzawa, H. Miki, F. Mignone, S. Miyake, K. Morris, S. Mottagui-Tabar, N. Mulder, N. Nakano, H. Nakauchi, P. Ng, R. Nilsson, S. Nishiguchi, S. Nishikawa, F. Nori, O. Ohara, Y. Okazaki, V. Orlando, K. C. Pang, W. J. Pavan, G. Pavesi, G. Pesole, N. Petrovsky, S. Piazza, J. Reed, J. F. Reid, B. Z. Ring, M. Ringwald, B. Rost, Y. Ruan, S. L. Salzberg, A. Sandelin, C. Schneider, C. Schönbach, K. Sekiguchi, C. A. M. Semple, S. Seno, L. Sessa, Y. Sheng, Y. Shibata, H. Shimada, K. Shimada, D. Silva, B. Sinclair, S. Sperling, E. Stupka, K. Sugiura, R. Sultana, Y. Takenaka, K. Taki, K. Tammoja, S. L. Tan, S. Tang, M. S. Taylor, J. Tegner, S. A. Teichmann, H. R. Ueda, E. van Nimwegen, R. Verardo, C. L. Wei, K. Yagi, H. Yamanishi, E. Zabarovsky, S. Zhu, A. Zimmer, W. Hide, C. Bult, S. M. Grimmond, R. D. Teasdale, E. T. Liu, V. Brusic, J. Quackenbush, C. Wahlestedt, J. S. Mattick, D. A. Hume, C. Kai, D. Sasaki, Y. Tomaru, S. Fukuda, M. Kanamori-Katayama, M. Suzuki, J. Aoki, T. Arakawa, J. Iida, K. Imamura, M. Itoh, T. Kato, H. Kawaji, N. Kawagashira, T. Kawashima, M. Kojima, S. Kondo, H. Konno, K. Nakano, N. Ninomiya, T. Nishio, M. Okada, C. Plessy, K. Shibata, T. Shiraki, S. Suzuki, M. Tagami, K. Waki, A. Watahiki, Y. Okamura-Oho, H. Suzuki, J. Kawai, Y. Hayashizaki; FANTOM Consortium; RIKEN Genome Exploration Research Group and Genome Science Group (Genome Network Project Core Group), The transcriptional landscape of the mammalian genome. *Science* **309**, 1559–1563 (2005).
8. D. S. Neems, A. G. Garza-Gongora, E. D. Smith, S. T. Kosak, Topologically associated domains enriched for lineage-specific genes reveal expression-dependent nuclear topologies during myogenesis. *Proc. Natl. Acad. Sci. U.S.A.* **113**, E1691–E1700 (2016).
9. K. Poterlowicz, J. L. Yarker, I. Malashchuk, B. R. Lajoie, A. N. Mardaryev, M. R. Gdula, A. A. Sharov, T. Kohwi-Shigematsu, V. A. Botchkarev, M. Y. Fessing, 5C analysis of the epidermal differentiation complex locus reveals distinct chromatin interaction networks between gene-rich and gene-poor TADs in skin epithelial cells. *PLOS Genet.* **13**, e1006966 (2017).
10. J. Dekker, M. A. Marti-Renom, L. A. Mirny, Exploring the three-dimensional organization of genomes: Interpreting chromatin interaction data. *Nat. Rev. Genet.* **14**, 390–403 (2013).
11. M. Rousseau, J. L. Crutchley, H. Miura, M. Suderman, M. Blanchette, J. Dostie, Hox in motion: Tracking HoxA cluster conformation during differentiation. *Nucleic Acids Res.* **42**, 1524–1540 (2014).
12. J. Arand, D. Spieler, T. Karius, M. R. Branco, D. Meilinger, A. Meissner, T. Jenuwein, G. Xu, H. Leonhardt, V. Wolf, J. Walter, In vivo control of CpG and non-CpG DNA methylation by DNA methyltransferases. *PLOS Genet.* **8**, e1002750 (2012).
13. J. P. Scott-Browne, C. J. Lio, A. Rao, TET proteins in natural and induced differentiation. *Curr. Opin. Genet. Dev.* **46**, 202–208 (2017).
14. A. Parry, S. Rulands, W. Reik, Active turnover of DNA methylation during cell fate decisions. *Nat. Rev. Genet.* **22**, 59–66 (2021).
15. G. L. Xu, M. Bochtler, Reversal of nucleobase methylation by dioxygenases. *Nat. Chem. Biol.* **16**, 1160–1169 (2020).
16. C.-W. J. Lio, Y. Xiaojing, I. F. Lopez-Moyado, M. Tahiliani, L. Aravind, A. Rao, TET methylcytosine oxidases: New insights from a decade of research. *J. Biosci.* **45**, 21 (2020).
17. L. Rinaldi, D. Datta, J. Serrat, L. Morey, G. Solanas, A. Avgustinova, E. Blanco, J. I. Pons, D. Matallanas, A. von Kriegsheim, L. di Croce, S. A. Benitah, Dnmt3a and Dnmt3b associate with enhancers to regulate human epidermal stem cell homeostasis. *Cell Stem Cell* **19**, 491–501 (2016).
18. N. Martin, S. Patel, J. A. Segre, Long-range comparison of human and mouse Sprr loci to identify conserved noncoding sequences involved in coordinate regulation. *Genome Res.* **14**, 2430–2438 (2004).
19. T. M. Magin, P. Vijayaraj, R. E. Leube, Structural and regulatory functions of keratins. *Exp. Cell Res.* **313**, 2021–2032 (2007).
20. V. A. Botchkarev, M. R. Gdula, A. N. Mardaryev, A. A. Sharov, M. Y. Fessing, Epigenetic regulation of gene expression in keratinocytes. *J. Invest. Dermatol.* **132**, 2505–2521 (2012).
21. J. Schweizer, P. E. Bowden, P. A. Coulombe, L. Langbein, E. B. Lane, T. M. Magin, L. Maltais, M. B. Omary, D. A. D. Parry, M. A. Rogers, M. W. Wright, New consensus nomenclature for mammalian keratins. *J. Cell Biol.* **174**, 169–174 (2006).
22. R. R. Driskell, C. A. Jahoda, C. M. Chuong, F. M. Watt, V. Horsley, Defining dermal adipose tissue. *Exp. Dermatol.* **23**, 629–631 (2014).
23. C. Blanpain, E. Fuchs, Epidermal homeostasis: A balancing act of stem cells in the skin. *Nat. Rev. Mol. Cell Biol.* **10**, 207–217 (2009).
24. M. I. Koster, D. Dai, D. R. Roop, Conflicting roles for p63 in skin development and carcinogenesis. *Cell Cycle* **6**, 269–273 (2007).
25. J. Schweizer, L. Langbein, M. A. Rogers, H. Winter, Hair follicle-specific keratins and their diseases. *Exp. Cell Res.* **313**, 2010–2020 (2007).
26. C. Bock, I. Beerman, W. H. Lien, Z. D. Smith, H. Gu, P. Boyle, A. Gnirke, E. Fuchs, D. J. Rossi, A. Meissner, DNA methylation dynamics during in vivo differentiation of blood and skin stem cells. *Mol. Cell* **47**, 633–647 (2012).
27. E. Ezhkova, W. H. Lien, N. Stokes, H. A. Pasolli, J. M. Silva, E. Fuchs, EZH1 and EZH2 cogovern histone H3K27 trimethylation and are essential for hair follicle homeostasis and wound repair. *Genes Dev.* **25**, 485–498 (2011).
28. J. Li, T. X. Jiang, M. W. Hughes, P. Wu, J. Yu, R. B. Widelitz, G. Fan, C. M. Chuong, Progressive alopecia reveals decreasing stem cell activation probability during aging of mice with epidermal deletion of DNA methyltransferase 1. *J. Invest. Dermatol.* **132**, 2681–2690 (2012).
29. R. Sennett, Z. Wang, A. Rezza, L. Grisanti, N. Roitershtein, C. Sicchio, K. W. Mok, N. J. Heitman, C. Clavel, A. Ma'ayan, M. Rendl, An integrated transcriptome atlas of embryonic hair follicle progenitors, their niche, and the developing skin. *Dev. Cell* **34**, 577–591 (2015).
30. A. Asare, J. Levorse, E. Fuchs, Coupling organelle inheritance with mitosis to balance growth and differentiation. *Science* **355**, eaah4701 (2017).
31. A. R. Folgueras, X. Guo, H. A. Pasolli, N. Stokes, L. Polak, D. Zheng, E. Fuchs, Architectural niche organization by LHX2 is linked to hair follicle stem cell function. *Cell Stem Cell* **13**, 314–327 (2013).
32. A. N. Mardaryev, N. Meier, K. Poterlowicz, A. A. Sharov, T. Y. Sharova, M. I. Ahmed, V. Rapisarda, C. Lewis, M. Y. Fessing, T. M. Ruenger, J. Bhawan, S. Werner, R. Paus, V. A. Botchkarev, Lhx2 differentially regulates Sox9, Tcf4 and Lgr5 in hair follicle stem cells to promote epidermal regeneration after injury. *Development* **138**, 4843–4852 (2011).
33. H. Rhee, L. Polak, E. Fuchs, Lhx2 maintains stem cell character in hair follicles. *Science* **312**, 1946–1949 (2006).
34. M. M. Dawlaty, A. Breiling, T. le, M. I. Barrasa, G. Raddatz, Q. Gao, B. E. Powell, A. W. Cheng, K. F. Faull, F. Lyko, R. Jaenisch, Loss of Tet enzymes compromises proper differentiation of embryonic stem cells. *Dev. Cell* **29**, 102–111 (2014).
35. M. M. Dawlaty, K. Ganz, B. E. Powell, Y. C. Hu, S. Markoulaki, A. W. Cheng, Q. Gao, J. Kim, S. W. Choi, D. C. Page, R. Jaenisch, Tet1 is dispensable for maintaining pluripotency and its loss is compatible with embryonic and postnatal development. *Cell Stem Cell* **9**, 166–175 (2011).
36. T. P. Gu, F. Guo, H. Yang, H. P. Wu, G. F. Xu, W. Liu, Z. G. Xie, L. Shi, X. He, S. G. Jin, K. Iqbal, Y. G. Shi, Z. Deng, P. E. Szabó, G. P. Pfeifer, J. Li, G. L. Xu, The role of Tet3 DNA dioxygenase in epigenetic reprogramming by oocytes. *Nature* **477**, 606–610 (2011).
37. K. Moran-Crusio, L. Reavie, A. Shih, O. Abdel-Wahab, D. Ndiaye-Lobry, C. Lobry, M. E. Figueroa, A. Vasanthakumar, J. Patel, X. Zhao, F. Perna, S. Pandey, J. Madzo, C. Song, Q. Dai, C. He, S. Ibrahim, M. Beran, J. Zavadil, S. D. Nimer, A. Melnick, L. A. Godley, I. Aifantis, R. L. Levine, Tet2 loss leads to increased hematopoietic stem cell self-renewal and myeloid transformation. *Cancer Cell* **20**, 11–24 (2011).
38. F. Santos, J. Peat, H. Burgess, C. Rada, W. Reik, W. Dean, Active demethylation in mouse zygotes involves cytosine deamination and base excision repair. *Epigenetics Chromatin* **6**, 39 (2013).
39. H. Q. Dai, B. A. Wang, L. Yang, J. J. Chen, G. C. Zhu, M. L. Sun, H. Ge, R. Wang, D. L. Chapman, F. Tang, X. Sun, G. L. Xu, TET-mediated DNA demethylation controls gastrulation by regulating Lefty-Nodal signalling. *Nature* **538**, 528–532 (2016).
40. D. B. Galbraith, Cell mass, hair type and expression of the agouti gene. *Nature* **222**, 288–290 (1969).
41. A. A. Sharov, T. Y. Sharova, A. N. Mardaryev, A. T. di Vignano, R. Atoyan, L. Weiner, S. Yang, J. L. Brissette, G. P. Dotto, V. A. Botchkarev, Bone morphogenetic protein signaling

regulates the size of hair follicles and modulates the expression of cell cycle-associated genes. *Proc. Natl. Acad. Sci. U.S.A.* **103**, 18166–18171 (2006).
42. N. V. Zernov, M. Y. Skoblov, A. V. Marakhonov, Y. Shimomura, T. A. Vasilyeva, F. A. Konovalov, A. V. Abrukova, R. A. Zinchenko, Autosomal recessive hypotrichosis with woolly hair caused by a mutation in the keratin 25 gene expressed in hair follicles. *J. Invest. Dermatol.* **136**, 1097–1105 (2016).
43. J. A. Nowak, E. Fuchs, Isolation and culture of epithelial stem cells. *Methods Mol. Biol.* **482**, 215–232 (2009).
44. J. R. Dixon, S. Selvaraj, F. Yue, A. Kim, Y. Li, Y. Shen, M. Hu, J. S. Liu, B. Ren, Topological domains in mammalian genomes identified by analysis of chromatin interactions. *Nature* **485**, 376–380 (2012).
45. R. E. Thurman, E. Rynes, R. Humbert, J. Vierstra, M. T. Maurano, E. Haugen, N. C. Sheffield, A. B. Stergachis, H. Wang, B. Vernot, K. Garg, S. John, R. Sandstrom, D. Bates, L. Boatman, T. K. Canfield, M. Diegel, D. Dunn, A. K. Ebersol, T. Frum, E. Giste, A. K. Johnson, E. M. Johnson, T. Kutyavin, B. Lajoie, B. K. Lee, K. Lee, D. London, D. Lotakis, S. Neph, F. Neri, E. D. Nguyen, H. Qu, A. P. Reynolds, V. Roach, A. Safi, M. E. Sanchez, A. Sanyal, A. Shafer, J. M. Simon, L. Song, S. Vong, M. Weaver, Y. Yan, Z. Zhang, Z. Zhang, B. Lenhard, M. Tewari, M. O. Dorschner, R. S. Hansen, P. A. Navas, G. Stamatoyannopoulos, V. R. Iyer, J. D. Lieb, S. R. Sunyaev, J. M. Akey, P. J. Sabo, R. Kaul, T. S. Furey, J. Dekker, G. E. Crawford, J. A. Stamatoyannopoulos, The accessible chromatin landscape of the human genome. *Nature* **489**, 75–82 (2012).
46. J. Hwang, T. Mehrani, S. E. Millar, M. I. Morasso, Dlx3 is a crucial regulator of hair follicle differentiation and cycling. *Development* **135**, 3149–3159 (2008).
47. P. Zhou, C. Byrne, J. Jacobs, E. Fuchs, Lymphoid enhancer factor 1 directs hair follicle patterning and epithelial cell fate. *Genes Dev.* **9**, 700–713 (1995).
48. G. Tornqvist, A. Sandberg, A. C. Hagglund, L. Carlsson, Cyclic expression of lhx2 regulates hair formation. *PLOS Genet.* **6**, e1000904 (2010).
49. V. A. Botchkarev, The molecular revolution in cutaneous biology: Chromosomal territories, higher-order chromatin remodeling, and the control of gene expression in keratinocytes. *J. Invest. Dermatol.* **137**, e93–e99 (2017).
50. S. Tanaka, I. Miura, A. Yoshiki, Y. Kato, H. Yokoyama, A. Shinogi, H. Masuya, S. Wakana, M. Tamura, T. Shiroishi, Mutations in the helix termination motif of mouse type I IRS keratin genes impair the assembly of keratin intermediate filament. *Genomics* **90**, 703–711 (2007).
51. B. K. Kim, H. Y. Lee, J. H. Choi, J. K. Kim, J. B. Yoon, S. K. Yoon, Hairless plays a role in formation of inner root sheath via regulation of Dlx3 gene. *J. Biol. Chem.* **287**, 16681–16688 (2012).
52. P. Nieminen, P. L. Lukinmaa, H. Alapulli, M. Methuen, T. Suojärvi, S. Kivirikko, J. Peltola, M. Asikainen, S. Alaluusua, DLX3 homeodomain mutations cause tricho-dento-osseous syndrome with novel phenotypes. *Cells Tissues Organs* **194**, 49–59 (2011).
53. M. Bochtler, A. Kolano, G. L. Xu, DNA demethylation pathways: Additional players and regulators. *Bioessays* **39**, 1–13 (2017).
54. S. Chrysanthou, Q. Tang, J. Lee, S. J. Taylor, Y. Zhao, U. Steidl, D. Zheng, M. M. Dawlaty, The DNA dioxygenase Tet1 regulates H3K27 modification and embryonic stem cell biology independent of its catalytic activity. *Nucleic Acids Res.* **50**, 3169–3189 (2022).
55. K. Ito, J. Lee, S. Chrysanthou, Y. Zhao, K. Josephs, H. Sato, J. Teruya-Feldstein, D. Zheng, M. M. Dawlaty, K. Ito, Non-catalytic roles of Tet2 are essential to regulate hematopoietic stem and progenitor cell homeostasis. *Cell Rep.* **28**, 2480–2490.e4 (2019).
56. Q. Shan, X. Li, X. Chen, Z. Zeng, S. Zhu, K. Gai, W. Peng, H. H. Xue, Tcf1 and Lef1 provide constant supervision to mature $CD8^+$ T cell identity and function by organizing genomic architecture. *Nat. Commun.* **12**, 5863 (2021).
57. V. A. Botchkarev, A. N. Mardaryev, Repressing the keratinocyte genome: How the polycomb complex subunits operate in concert to control skin and hair follicle development. *J. Invest. Dermatol.* **136**, 1538–1540 (2016).
58. A. A. Sharov, G. Z. Li, T. N. Palkina, T. Y. Sharova, B. A. Gilchrest, V. A. Botchkarev, Fas and c-kit are involved in the control of hair follicle melanocyte apoptosis and migration in chemotherapy-induced hair loss. *J. Invest. Dermatol.* **120**, 27–35 (2003).
59. J. D. Buenrostro, P. G. Giresi, L. C. Zaba, H. Y. Chang, W. J. Greenleaf, Transposition of native chromatin for fast and sensitive epigenomic profiling of open chromatin, DNA-binding proteins and nucleosome position. *Nat. Methods* **10**, 1213–1218 (2013).
60. N. C. Durand, M. S. Shamim, I. Machol, S. S. P. Rao, M. H. Huntley, E. S. Lander, E. L. Aiden, Juicer provides a one-click system for analyzing loop-resolution Hi-C experiments. *Cell Syst.* **3**, 95–98 (2016).

Acknowledgments: We thank W. Reik (Babraham Institute, UK) for providing *Tet3* floxed mice for this study and Director of Cell Sorting Core Facility B. R. Tilton (Boston University School of Medicine, USA) for technical support during fluorescence-based cell enrichment. **Funding:** This work was supported by the National Institutes of Health grant 5R01 AR075776 (V.A.B. and A.A.S.) and grant 5R01 AR071727 (V.A.B. and A.A.S.) and the National Science Foundation of China (G.-L.X.). **Author contributions:** Conceptualization: G.-D.C., G.-L.X., M.Y.F., and V.A.B. Methodology: G.-D.C., M.Y.F., and A.A.S. Investigation: G.-D.C., A.N.M., Q.X., I.F., E.R., and A.A.S. Supervision: G.-L.X., A.A.S., and V.A.B. Writing—original draft: G.-D.C. and V.A.B. Writing—review and editing: G.-D.C., G.-L.X., M.Y.F., A.A.S., and V.A.B. **Competing interests:** The authors declare that they have no competing interests. **Data and materials availability:** The following sequencing data were deposited into the GEO database (accession numbers for RNA-seq and CUT&Tag data: GSE212825; for WGBS: GSE212791: and for Hi-C data: GSE212455). All other data needed to evaluate the conclusions in the paper are present in the paper and/or the Supplementary Materials.

Submitted 25 February 2022
Accepted 5 December 2022
Published 11 January 2023
10.1126/sciadv.abo7605